An atypical basement membrane forms a midline barrier during left-right asymmetric gut development in the chicken embryo

Cora Demler[1], John Coates Lawlor[1], Ronit Yelin[2], Dhana Llivichuzcha-Loja[1], Lihi Shaulov,[3] David Kim[1], Megan Stewart[1], Frank Lee*, Natalia A. Shylo[4], Paul A. Trainor[4,5], Thomas Schultheiss[2], Natasza A. Kurpios[1+]

[1]Department of Molecular Medicine, College of Veterinary Medicine, Cornell University, Ithaca, NY 14853, USA
[2]Department of Genetics and Developmental Biology, Rappaport Faculty of Medicine, Technion-Israel Institute of Technology, Haifa 31096, Israel
[3]Rappaport Faculty of Medicine, Technion-Israel Institute of Technology, Haifa 31096, Israel
*Deceased
[4]Stowers Institute for Medical Research, Kansas City, MO, USA
[5]Department of Anatomy and Cell Biology, University of Kansas Medical Center, Kansas City, Missouri, USA

[+]Corresponding author, natasza.kurpios@cornell.edu.

Abstract

Correct intestinal morphogenesis depends on the early embryonic process of gut rotation, an evolutionarily conserved program in which a straight gut tube elongates and forms into its first loops. However, the gut tube requires guidance to loop in a reproducible manner. The dorsal mesentery (DM) connects the gut tube to the body and directs the lengthening gut into stereotypical loops via left-right (LR) asymmetric cellular and extracellular behavior. The LR asymmetry of the DM also governs blood and lymphatic vessel formation for the digestive tract, which is essential for prenatal organ development and postnatal vital functions including nutrient absorption. Although the genetic LR asymmetry of the DM has been extensively studied, a divider between the left and right DM has yet to be identified. Setting up LR asymmetry for the entire body requires a *Lefty1*+ midline barrier to separate the two sides of the embryo, without it, embryos have lethal or congenital LR patterning defects. Individual organs including the brain, heart, and gut also have LR asymmetry, and while the consequences of left and right signals mixing are severe or even lethal, organ-specific mechanisms for separating these signals are poorly understood. Here, we uncover a midline structure composed of a transient double basement membrane, which separates the left and right halves of the embryonic chick DM during the establishment of intestinal and vascular asymmetries. Unlike other basement membranes of the DM, the midline is resistant to disruption by intercalation of Netrin4 (Ntn4). We propose that this atypical midline forms the boundary between left and right sides and functions as a barrier necessary to establish and protect organ asymmetry.

Key words: left-right asymmetry, midline barrier, organogenesis, gut, basement membrane, laminin, dorsal mesentery

Introduction

Humans and most other animals are bilaterians—animals whose left and right external features can be mirrored—but often the internal organs have striking LR asymmetries. For example, in humans the heart resides on the left side of the thoracic cavity, the liver is predominantly on the right, and the spleen is on the left. Even paired organs like the lungs can show LR asymmetries—the left human lung has two lobes while the right lung has three. The left and right sides of the body are specified early in development, after the anterior/posterior and dorsal/ventral axes have been established.[1,2] This patterning relies heavily on the expression of Sonic hedgehog (*Shh*) upstream of Nodal on the left side, and the repression of these genes by Activin on the right side.[3] The localization of SHH-producing cells to the left is accomplished by nodal flow (mouse,[4,5] zebrafish[6] and *Xenopus*[7] embryos) or rotational cell movements around the node (chicken and pig embryos),[8] as well as cell death at the embryonic midline that may be a consequence of its abundant extracellular matrix (ECM).[9]

Establishing the vertebrate LR body axis depends on a midline barrier to separate side-specific diffusible signals.[10–15] This is achieved with a highly specific expression pattern of an inhibitor, Lefty1, at the center of the embryo which prevents the diffusible, left-sided signal NODAL from crossing to the embryo's right side.[11–15] Sixty percent of Lefty1-knockout mouse embryos die in utero and an additional 20% die before weaning, suffering from left isomerism of the lungs (in other words, both lungs have left lung lobation) and positional defects of the heart and the major vessels leading into/out of it.[13] Other important examples of laterality defects are seen in conjoined twins, in which an embryo divides partially at the primitive streak stage (Day 13-14 of gestation for humans).[16] In laterally conjoined (dicephalus) twins which form when the two primitive streaks are parallel, the left side of one embryo and the right side of the other are connected without the LEFTY1 barrier in between. Consequently, these conjoined twins often exhibit LR defects.[17,18]

This underscores that separation of left and right signals is fundamental in early development for setting up correct placement and LR asymmetric patterning of individual organs including the heart and gut.[6,10,19–21] Of all the organs with LR asymmetry, only the brain is known to harbor an organ-specific midline barrier.[22–28] Thus, midline barriers may have broad developmental significance for the embryo and its organs, yet very few such structures have been characterized.

Even organs that do not have obvious LR differences in the adult develop as a result of conserved LR asymmetric morphogenesis. The intestine is an excellent model for this, especially given the relatively simple tubular structure of the organ itself. During development, the intestine grows to great lengths (about eight meters in adult humans),[29] and this long tube must be looped to fit into the body cavity in a stereotypical, species-specific way.[30,31] When the developmental program directing gut looping is perturbed, as is the case for one in 500 infants who have congenital malrotation of the gut, there is an increased risk of volvulus, a lethal self-strangulation of the gut that requires immediate pediatric surgical intervention.[32]

The gut tube does not loop autonomously. Rather, gut looping is directed by the neighboring dorsal mesentery (DM) (Fig. 1A), a thin mesodermal organ that connects the gut to the rest of the body and through which intestinal blood and lymphatic vessels traverse.[31,33–35] The left and right sides of the DM take on different properties at the molecular, cellular, and extracellular levels which are critical to initiate asymmetric gut looping and vascular morphogenesis.[33,36–40] Gut tilting is the symmetry-breaking event that initiates asymmetric gut looping, which occurs at embryonic day 10.5 (E10.5) in the mouse and Hamburger-Hamilton stage 19-21 (HH19-21)[41] in the chicken embryo (Fig. 1B).[37] Gut tilting is driven by the condensation of the ECM in the left DM, and an expansion of the ECM on the right (Fig. 1B).[36] Blood vasculature also develops asymmetrically. Although endothelial precursors exist on both the left and right DM prior to tilting, as the asymmetries are established the right-sided endothelial

cells emigrate rather than forming vessels.[33] Only a left-sided gut artery develops further (Fig. 1B), which goes on to supply blood to a significant portion of the adult intestine (Fig. 1A).[33] Interestingly, these right-sided endothelial cells emigrate dorsally and ventrally, but they cannot cross directly over to the left side.[33] This might indicate the presence of a barrier against cell migration at the midline.

The differences in the left and right sides of the DM are well understood at multiple levels of biology, but the maintenance of these asymmetries has not been explored. The classes of genes with asymmetric expression in the DM include transcription factors, ECM components, and genes which encode diffusible signals that could spread within the DM compartments to create morphogen gradients across the LR axis. Instead of a LR gradient, however, there is a sharp delineation between left and right DM in gene expression and protein localization, as well as LR asymmetric distribution of extracellular glycosaminoglycans, such as hyaluronan.[33,36–40] Not surprisingly, perturbing even just one gene's asymmetric expression patterns in the DM leads to aberrant gut looping patterns and abnormal vascular lesions.[33,38–40] Thus, we hypothesized that a barrier exists in the center of the DM to segregate cells and diffusible signals to the left and right compartments. Here, we show that an atypical basement membrane forms a boundary between left and right cell populations and limits diffusion across the DM midline.

Results

Cells of left- and right-origin meet but do not mix in the DM

The DM mesenchyme forms by bilateral epithelial-to-mesenchymal transition (EMT) and ingression of coelomic epithelium, which is derived from the splanchnic mesoderm; the left DM comes from the left coelom and the right DM arises from the right coelom (Fig. 2A and B).[35–37] This was visualized by injecting early chicken embryos with DiI and DiO into the right and left

coelomic cavities, respectively (Fig. 2C-F), or by electroporating each side with plasmids encoding different fluorophores (Fig. 2G and H). While the left and right cells meet at the middle of the DM, they never cross over or mix.[33,36–38,40,42–45] This striking separation occurs despite the lack of a visible histological boundary between the two sides as shown by H&E staining at HH20 and HH21, when the left is condensing and the right is expanding to drive the leftward gut tilting (Fig. 2K and L). Early in development the endoderm effectively separates the left and right splanchnic mesoderm (Fig. 2I and J), but once the DM forms and the endoderm descends it is likely important to continue separating the two sides until asymmetries can be established (Fig. 1B). In support of this, we have previously shown that when cell-cell adhesion is interrupted in the left DM, the cells become more dispersed[36,38] and extend filopodia over towards the right side, suggesting pathogenic cell migration.[38] Thus, the critical separation between left and right cells in the DM can be disrupted, necessitating a mechanism for protecting these asymmetries.

The DM midline is not marked by Lefty1, but by laminin

The early embryo uses a molecular barrier of *Lefty1*-expressing cells to separate laterality signals so the LR axis is established correctly.[11–15] To see if this mechanism is adapted by the intestine for establishment of its laterality, we performed *Lefty1* RNA *in situ* hybridization on both early (HH9) and later (HH19) stages. While *Lefty1* was expressed at the midline of early embryos as expected (Fig. 3A), it was not expressed at the midline of the DM at HH19 (Fig. 3B). This indicates that a different mechanism must be at work during the establishment of gut asymmetries. Interestingly, scanning electron microscopy (SEM) data showed a fibrous matrix between the notochord and endoderm where the DM will later develop, suggesting that ECM may separate the two sides before they coalesce into the DM (Fig. 3C and D). Consistent with this hypothesis, basement membranes are found in other biological contexts where a barrier is needed, such as

in the skin or around blood vessels.[46] Basement membranes are dense ECM requiring laminin, collagen IV, nidogen, and perlecan and/or agrin (both heparan sulfate proteoglycans) with a large variety of other components that can be integrated to create specific “flavors" of basement membrane tuned to different barrier contexts.[46] We therefore postulated that the DM midline has a physical barrier consisting of basement membrane, rather than a *Lefty1* molecular barrier.

To test this hypothesis, we visualized the basement membrane marker laminin by immunofluorescence (IF) for laminin alpha 1 (Lama1) at developmental stages where DM asymmetries are being established. As expected, this marked several typical, single-layer basement membranes underlying polarized cells, such as around the notochord (Fig. 3E and F),[47,48] coelomic epithelium (Fig. 3E-H),[49] and gut endoderm (Fig. 3E-H).[50] We also observed scattered laminin staining in the DM mesenchyme, which is a consequence of those cells carrying basement membrane fragments with them after EMT and ingression from the coelomic epithelium.[51,52] Interestingly, we identified a previously uncharacterized atypical double basement membrane within the DM. At HH18, when cellular DM asymmetries are first being initiated at the level of the midgut (which forms the small intestine), laminin IF marked an oval-shaped structure just ventral to the notochord and dorsal to the gut endoderm (Fig. 3E). No cells were seen within this structure as shown by a lack of nuclear staining (Fig. 3E) and empty space in SEM (Fig. 3C and D, S1C). As the DM elongates and asymmetries become more apparent (HH19), this midline structure lengthened, forming two parallel lines connecting the endoderm and notochord (Fig. 3F). One stage later (HH20), the midline was still present but began to appear fragmented (Fig. 3G). By HH21, the asymmetries of the DM are established—the right DM has expanded, the left DM has condensed, the gut has tilted to the left, and vascular precursor cells have been driven out of the right side (Fig. 1B).[33,40,43] Surprisingly, the midline disappeared by this stage, while laminin IF underlying the coelomic epithelium and endoderm remained intense (Fig. 3H). The lengthening

of the midline and its subsequent loss occurred in an anterior-to-posterior wave down the embryonic gut tube (Fig. 3J and K). Consequently, anterior sections of younger embryos (i.e., HH12-13) had similar midline structures to posterior, older sections (i.e., HH18-19) (compare Fig. S2E-H with S2A-D).

The DM midline consists of a transient, true basement membrane

The combination of laminin, nidogen, perlecan (or agrin), and collagen is the foundation of all basement membranes.[46] To further characterize the nature of the ECM at the DM midline, we did IF staining for nidogen and perlecan, confirming co-localization with laminin at the midline barrier (Fig. S3A, S3B). This further illustrates that the DM midline consists of basement membrane. This basement membrane structure is conserved in the squamate veiled chameleon, *Chamaeleo calyptratus*, which exhibits a similarly transient double basement membrane at the midline of the dorsal mesentery from approximately the 7-somite stage to the 29-somite stage (Fig. S5).[53]

In addition to the four foundational basement membrane components, a myriad of other proteins, proteoglycans, and glycoproteins can assemble onto the basement membrane.[54] Consequently, there is a vast variety of “flavors” of basement membrane with different physical properties and different signals to adjacent cells about polarity, migration, or other behaviors.[54] A common basement membrane constituent is fibronectin, which is best known for its role in the provisional matrix during wound healing.[55] At our developmental stages of interest, fibronectin localized to the dorsal aorta which often coincides with the most ventral part of the midline (Fig. S2, S3C). Together, we model the midline as a transient double basement membrane that bisects the DM during developmental stages when critical asymmetries are being established (Fig. 3L).

The midline does not originate from the left or right DM

Although we have established the time kinetics of DM midline formation, the origin of this structure remains elusive. The midline is sandwiched between mesenchymal cells from the left and right DM, unbiased to either the left or the right side (Fig. 2F and G). Intriguingly, mesenchymal cells like these are not usually competent to construct an organized basement membrane.[46,56] Mesenchymal cells can secrete matrix components,[50] but the organization of these components into a basement membrane is dependent on the presence of cell surface anchors which are characteristic of tissues like polarized epithelium or endothelium, not mesenchymal cells.[56] In the case of LAMA1, it is known that this protein is secreted by the epithelia in the developing intestine, not the mesenchyme.[50] Indeed, RNA *in situ* hybridization for *Lama1* did not show enriched expression in the mesenchyme at the DM midline (Fig. 4B and C). Moreover, if the cells adjacent to the midline were secreting and organizing the basement membrane, we would expect these cells to be polarized like the cells of the coelomic epithelium or endoderm. As expected, the left coelomic epithelium was polarized at HH19 relative to its basement membrane as quantified by Golgi staining with GM130 (Fig. 4D and E).[38] However, GM130 staining and quantification showed that cells immediately to the left or right of the midline have random orientation (Fig. 4D and E). Together, these data allow us to rule out a mesenchymal origin for the DM midline.

<u>During endodermal descent, endodermal cells are not left behind to form the midline</u>

Given that the DM midline connects the notochord and endoderm, both of which have their own basement membranes and are very closely associated early in development, we hypothesized that one or both of these structures contributes to midline production (Fig. 3C/E/J, S1A). As the embryo grows and the DM elongates, the distance between the notochord and endoderm increases (Fig. 2I-J, 3E-H), and the midline is found between them as a double line of basement membrane. Thus, we hypothesized that as the endoderm descends ventrally, it undergoes EMT

and leaves behind basement membrane-carrying cells to form the midline. To test this, we developed a method to specifically target the endoderm using DNA electroporation (Fig. 4F). Briefly, we injected pCAG-GFP plasmid underneath HH14-15 embryos and applied an electric pulse such that the endodermal cells would take up the DNA (Fig. 4F), so we could lineage trace endodermal cells during DM formation. Interestingly, embryos isolated at HH19 and HH21 showed that GFP-labeled cells remain restricted to the endoderm—there were no GFP+ mesenchymal cells present in the DM (Fig. 4G, H). This indicates that the DM midline is not formed from EMT of basement membrane-carrying endodermal cells.

The notochord is not sufficient for DM midline formation

To test whether the notochord is sufficient for midline formation, we performed notochord transplant experiments. In brief, the notochord was removed from an HH12-15 embryo. An incision was made in a stage-matched recipient embryo adjacent to the neural tube and the donor notochord was inserted into this slit (Fig. 4I). Embryos continued to develop until isolation at HH19. These transplants were done to the left and right sides of different embryos (Fig. 4J/K and 4L/M respectively). RNA *in situ* hybridization was performed for *chordin* to ensure that the transplanted notochord was alive and functioning (Fig. 4J and L).[57,58] Laminin IF did not reveal a secondary midline-like structure associated with the ectopic notochord (Fig. 4K and M) while the normal midline was unaffected (Fig. 4K and M, white arrows). This result is seen regardless of whether the transplants are done to the embryo's left or right side. From this, we conclude that the notochord is not sufficient for the formation of DM midline.

The DM midline is resistant to degradation by Netrin4

Laminin matrices are susceptible to competitive disruption by the matrix protein Netrin4 (NTN4).[59,60] NTN4 has very high binding affinity for laminin gamma subunits, such that NTN4 can prevent the formation of new laminin networks, which are the foundation upon which other basement membrane components assemble, and can also disrupt existing laminin networks.[59,60] *Ntn4* is not endogenously expressed in the DM (data not shown), which allows us to use it as a tool to target basement membranes in the DM. As expected, when we overexpressed *Ntn4* on either side of the DM by electroporation, we perturbed the basement membrane underlying the coelomic epithelium and depleted the scattered laminin staining in the mesenchyme that results from EMT creating the DM (Fig. 5B, D, and E vs. controls 5A and C).[51,52] Intriguingly, the DM midline basement membrane remained visibly intact in all embryos with lateral (Fig. 5B and D) and bilateral (Fig. 5E) *Ntn4* overexpression in the DM. Similarly, endodermal *Ntn4* overexpression caused much less disruption of the endodermal or midline basement membranes (Fig. 5G vs control 5F) when compared to its effect on coelomic epithelium basement membrane. This was true even when the electroporations were done much earlier in development (HH10 and HH12-13, data not shown). This suggests that the midline and endoderm may have basement membranes of the same "flavor," possibly pointing to a common origin. In contrast, the basement membrane beneath the coelomic epithelium may be more susceptible to NTN4 disruption because of the prior EMT-induced breaks in the basement membrane,[51,52] or a different protein composition.

<u>DM midline is a barrier against diffusion</u>

Genes including Cxcl12[33,39] and Bmp4[40] which encode diffusible signals are expressed asymmetrically in the DM (Fig. 6A and B). So too are genes encoding enzymes that are secreted into the ECM, like the HA-modifying enzyme TSG6.[39] The expression domains of these genes

have a sharp boundary at the midline, since left and right cells do not mix. However, the secreted protein products of these genes may be able to diffuse across the DM if their movement is not limited (Fig. 6C). We know that experimentally mixing left and right signals is detrimental to gut tilting and vascular patterning[33,36–40]—for example, ectopic expression of pro-angiogenic Cxcl12 on the right side results in an aberrant vessel forming on the right.[33] Moreover, when the CXCR4 receptor antagonist AMD3100 (MW=502.78) is introduced to the left DM, it abolishes vascular development on the left. However, when the same drug is introduced to the right DM, the left-sided vascular development remains intact.[33] This phenomenon suggests a barrier against diffusion.

To test if the basement membrane structure at the midline is forming a functional barrier against diffusion, we injected 3 kDa fluorescent dextran directly into the right side of the DM (Fig. 6D-G). When these injections are performed at stages where the midline is intact (HH19), movement of dextran through the tissue was limited to the right side (n = 4/4 embryos) (Fig. 6D). When the basement membrane midline appears fragmented (HH20), these injections produced mixed results—in some embryos (n = 2/9), diffusion across the midline was prevented and in others (n = 7/9) the dextran was able to move into the left mesenchyme of the DM (Fig. 6E). Finally, at stages where no organized basement membrane structure remains at the midline (HH23), diffusion of dextran was always permitted across the entire width of the DM (n = 7/7) (Fig. 6F).

To confirm our finding that the basement membrane structure at the midline forms a barrier against diffusion, we utilized a BODIPY-tagged version of AMD3100,[61] delivered via soaked resin beads surgically inserted into the left coelomic cavity (Fig. 6H-L). The ratio of average AMD3100-BODIPY intensity in the right DM versus the left DM was below 0.5 when the midline is intact (HH19, n = 4/4), indicating little diffusion across the DM (Fig. 6J). When no

midline remains at a later stage (HH21, n = 4/4), this ratio significantly rises to near one, indicating diffusion of the drug is not impeded when the midline basement membrane structure is absent (Fig. 6J). Collectively, these data suggest that the basement membrane structure at the midline forms a transient functional barrier against diffusion (Fig. 6M).

Discussion

Establishing the left and right body plan in the early embryo is a fundamental part of development and this process depends on the presence of a Lefty1+ midline barrier. Individual organs, too, have LR asymmetries, but the brain has the only known organ-specific midline barrier, where commissural axons of the brain and spinal cord are tightly controlled by midline-localized guidance and repulsion cues including FGFs, SLIT/ROBO signaling, EFNB3, heparan sulfate proteoglycans, and the Rac-specific GTPase-activating protein α-chimaerin.[22–28] The developing intestine has a similar need for separation between left and right cells and signals, but it seems to accomplish this by a different mechanism—an atypical basement membrane at the midline.

This basement membrane may separate cells that have ingressed from the right and left coelomic epithelia,[62] since these cells do not mix at the midline (Fig. 2). It may also prevent mixing of diffusible signals. While the diffusion of a given signal depends on the tissue context,[63] some morphogens (like Nodal) can induce effects at distances of 200 µm or greater.[64] The HH19 DM is only about 150 µm across, not a prohibitive distance for diffusible signals like BMPs, TGFß,[40] and CXCL12[33] to cross between the left and right DM. Thus, we hypothesized that the DM may need a barrier at the midline to segregate these signals. In support of this, we showed that the midline limits diffusion of dextran from right to left, which suggests that it also blocks the movement of endogenous diffusible signals. Moreover, with a molecular weight of just 3 kDa, dextran's inability to cross the midline indicates that diffusible proteins of typical weight (such as CXCL12

at 10 kDa and BMP4 at 34 kDa) are also unable to cross. We previously showed evidence that even the 502.78 Da drug AMD3100 was prevented from moving to the other side of the DM.[33] In line with these findings, we have now employed a BODIPY-labeled form of AMD3100[61]. Similar to dextran, our results show BODIPY diffusion across the midline when the basement membrane is intact. However, when no basement membrane remains at the midline, BODIPY diffusion was permitted across the entire DM width. While the midline could not be degraded by *Ntn4* overexpression, future studies may reveal tools for the selective destruction of this basement membrane to better understand its function in gut laterality.

This work adds a new facet to our knowledge of basement membrane form and function. Basement membranes play many critical barrier functions in the embryo and adult, usually found as a single layer that underlies polarized epithelial or endothelial cell layers such as those lining the intestines, encircling blood vessels, or enveloping muscle cells, adipocytes, or Schwann cells.[46] As such, null mutations in genes encoding basement membrane components often result in embryonic lethality and postnatal pathologies.[65–70] However, a role for basement membrane in establishing LR asymmetry has not been described previously.

The basement membrane we describe here is atypical in its double membrane structure, which raises interesting questions about its formation. We showed that the midline is not produced by the mesenchymal cells of the DM (Fig. 4), and that the notochord is not sufficient for its synthesis (Fig. 4). Instead, we consider the endoderm. Upon electroporation of the endoderm with GFP, GFP-positive cells were not detected in the DM later in development but remained restricted to the endoderm (Fig. 4F-H), indicating that the midline does not form from EMT of basement membrane-carrying endodermal cells. We can also eliminate endodermal death as a possible mechanism, because there was no appreciable cell death observed by TUNEL staining at the midline during the stages of interest (data not shown). Nor does the midline form in the same way

as other double basement membranes, which arise from the meeting of the basal sides of two tissues.[71,72] This is classically illustrated in the kidney glomerulus between epithelial podocytes and endothelial cells[72–74] and in the blood-brain barrier between endothelial cells, pericytes, and astrocytes.[71,75] Instead in the case of the DM midline barrier, the apical sides of the endodermal cells are facing each other.

We hypothesize that the midline forms when basement membrane is left behind as the endoderm descends ventrally during normal development, as if it were a “scar” of where the endoderm was previously (Fig. 7). During early development the notochord is embedded within the endoderm and a basement membrane covers the two structures. Only later are the two structures separated by a full basement membrane, pointing to a strong connection between the two.[76,77] The medial migration of the aortae and coelomic epithelia could provide tissue forces that push the notochord and endoderm apart, leaving behind basement membrane at the DM midline. The observation that the basement membranes of both the endoderm and midline were resistant to disruption by NTN4 could also support the idea that the endoderm is responsible for making both basement membranes (Fig. 7). In support of this, we know that the basement membrane underlying the gut endoderm does not co-migrate with the intestinal epithelial cells as they move from the proliferative intestinal crypts to the tip of the villus over the course of three to six days in the adult; the basement membrane is instead left in place.[78] One way to test this hypothesis would be to “trace” endodermal basement membrane by electroporation of a tagged basement membrane component, as has been done recently in *C. elegans*[79–84] and *Drosophila*.[85,86] However, these advances are only just now reaching the mouse system[87,88] and have not yet made their way into the chick embryo.

The endodermal basement membrane and midline's resistance to NTN4 disruption is particularly notable, as similar resistance has not been reported before. This suggests the

presence of an unknown factor or modification that shields or stabilizes the laminin network from NTN4 binding. Investigating the mechanisms that stabilize basement membranes against such disruptions could be important for future developmental studies and research on basement membranes in the context of disease and cancer.

Although Lefty1 expression is not observed at the midline when this basement membrane is robust, it remains unclear whether midline Lefty1 expression is crucial for the construction or proper function of this structure. Future research could involve siRNA inhibition of Lefty1 expression at an early stage, followed by an evaluation of the midline structure's integrity at HH19. However, similar to perturbing global Nodal expression, it may be challenging to differentiate between the direct impact of Lefty1 loss on future midline cells, and the indirect impact on midline cells resulting from free Nodal diffusion throughout the early lateral mesoderm that would happen as a consequence of Lefty deficiency. Further investigation into the relationship between these two aspects of the midline barrier is important.

The midline barrier is set apart from many other basement membranes by its rapid disappearance. We consider that the loss of the DM midline barrier may be caused in part by “stretching” of the basement membrane as the notochord and endoderm become increasingly separated due to the elongation of the DM (Fig. 3J). Since the DM itself does not contribute basement membrane to the midline (Fig. 4C) and the midline length increases quickly (Fig. 3J), it is plausible that the midline may be pulled until it reaches its ultimate tensile strength (between 0.5-3.8 MPa in other examples of naturally occurring basement membranes),[89] and then breaks. This would suggest that midline breakdown is a passive consequence of embryo growth.

However, we also consider that there could be an active breakdown mechanism for the midline. The turnover of stable basement membranes occurs on the scale of weeks,[78,90] but the midline barrier appears to degrade over just 12-24 hours. In other contexts, basement membrane destruction can occur over a large area, such as by secretion of matrix metalloproteinases

(MMPs) in metastasizing cancer,[91,92] or more localized, as exhibited by invadopodia on immune or cancer cells before metastasis.[93,94] Such localized basement membrane breakdown is seen in critical developmental processes, including mouth development in deuterostome embryos.[95] The oral membrane includes a basement membrane that closes off the digestive system from the outside world. This basement membrane specifically disintegrates to rupture that membrane to open the early mouth cavity.[95] In addition, a basement membrane divides the two halves of the embryonic brain, and must be broken down at the site of the corpus callosum for neurons to cross for inter-hemisphere communication in the cerebrum.[96,97] Localized basement membrane dissolution is also critical for optic cup fusion, where a contact-dependent dissolution of basement membrane occurs between the two sides of the optic fissure.[98,99] Coloboma, a congenital eye defect where some tissue is missing inside the eye resulting in an enlarged, irregular pupil, occurs when optic fusion arrests.[100,101] It is worth noting that in all of these examples and the case of the midline, the location of basement membrane breakdown is very specific—neighboring basement membranes appear unaffected (Fig. 3H). Together, these findings support the idea that basement membrane breakdown in the DM may not simply be a passive process but may be required by the embryo for later events in gut development or vascular patterning. We have not yet identified any matrix protease specific to the midline of the DM. Given that a mechanism for basement membrane breakdown is not well characterized in any of the above contexts, there is high potential for future investigation.

The DM midline may have effects on development beyond the intestine. It has long been known that signals produced from axial structures in the embryo are critical for the establishment of LR asymmetry, but it has been difficult for researchers to pin down which “midline structure” or “midline signal” is actually responsible. For example, the heart,[102,103] lungs,[44] and kidneys[104] all rely on “dorsal midline structures” to develop properly. Aberrations from the loss of midline

structures like the notochord include “horseshoe kidney,” in which the kidneys stay close to the midline and fuse at their posterior end.[105] This is due to the lack of notochordal Shh signaling, but the “midline barrier” that exists downstream from this Shh signaling remains a mystery.[106]

The DM midline barrier may also play a role in vascular patterning, including aortic fusion. The aorta begins as two parallel tubes with an avascular zone in between (where the midline is),[107] but progressively they fuse into one with an anterior-to-posterior wave until the level of the vitelline arteries (Fig. S2A-D).[107] Fusion of the aortae coincides with the fragmentation and disappearance of the midline, suggesting that these two processes may be inextricably linked (Fig. 3J, S2). Proper timing of this fusion depends on carefully balanced levels of VEGF,[108] SHH,[109] and the anterior-to-posterior wave of downregulation of the BMP-inhibitory genes Chordin and Noggin from the notochord.[107,110,111] The precise mechanism of dorsal aorta fusion remains unknown, although there is evidence that VEGF signaling pulls VE-cadherin away from its cell-cell junctions.[108] This relocalization may be important for the remodeling of the aortic endothelium during fusion and may be linked to the breaking of the DM midline barrier.

Midline structures are critical for laterality to develop correctly. The notochord is certainly involved, particularly as the source of modulators of BMP and Hedgehog signaling. However, this does not seem to be the whole story, given that in each of these contexts the actual “midline barrier” downstream from notochord signals has not been identified. It is possible that the DM midline basement membrane is key here, either for separating left and right signals or perhaps for binding signals[69] from the notochord to act as a buffer between each side. The midline barrier may also play a role in the rheology of the DM. Microindentation analyses at HH21 show that the condensed left DM is significantly stiffer than the expanded right DM, and that proper gut tilting is dependent on this difference being tightly regulated.[40] It is possible that the midline barrier helps to segregate the stiffness-influencing components of each side (i.e. covalently modified HA on

the right,[39] N-cadherin on the left[36]) and provides a “wall” for the right side to push upon in order to swing the gut tube towards the left. It's important to note that left and right mesenchymal cells do not cross the midline to the opposite side of the DM. Likewise, during the formation of gut arteries, a small subset of gut vascular endothelial cells migrate from right to left, closely adjacent to the dorsal tip of the endoderm, but they do not traverse the midline.[33] Moreover, when the midline basement membrane is present and intact, N-cadherin expression is symmetric across the DM, but becomes asymmetric and left-specific upon midline disintegration.[36] This may represent a shift in cell segregation mechanisms in the DM - while the midline is intact, the double basement membrane structure appears sufficient to segregate left and right cells. When the midline disappears, a new cellular separation mechanism is required to maintain asymmetric compartments, and N-cadherin functions in this role.

Looping patterns of the midgut are stereotypical between individuals but vary between species.[31] While differential growth rates between the gut tube and the dorsal mesentery have been identified as the primary means by which distinct gut looping patterns may be achieved,[31] it is also possible that mesentery-specific changes such as modifications to the kinetics of asymmetry in the DM may impact looping patterns with potentially adaptive impact on diet and therefore niche utilization. The presence, permeability, and timing of degradation of the midline basement membrane may provide evolution with an additional means of fine-tuning looping patterns between species. We have found this basement membrane to be transiently present in the DM of veiled chameleon embryos from just after the seven-somite stage to the 29-somite stage (Fig. S5),[53] suggesting this structure is conserved in reptiles and birds at a minimum, with intriguing heterochrony in degradation between species. In mammals, prior studies have observed midline laminin deposition in the mouse gut located between the separating notochord and endoderm, further suggesting conservation of a midline basement membrane in amniotes.[112,113]

Collectively, we have identified a novel midline barrier in the gut mesentery that is composed of an atypical double basement membrane that forms a boundary between the left and right sides and limits movement of diffusible signals and cells, at a stage when Lefty1 is no longer expressed at the midline. The DM midline also presents an opportunity to interrogate the fundamental mechanisms of basement membrane formation and degradation during vertebrate embryonic development, with implications for research on cancer metastasis. We posit that this midline is a distinct strategy for the critical separation of left and right signals and cells, key for establishing and maintaining LR asymmetry for healthy gut development.

Materials and Methods

Chicken embryo development and processing

Fertile chicken eggs were purchased from Westwind Farms (Interlaken, NY http://chickenhawkfood.com). After 36-48 hours of incubation at 37˚C, eggs were windowed by removing 8 mL of thin albumen with an 18 ½ gauge needle/10 mL syringe and cutting an oval in the side of the shell, then covering the opening with clear packing tape and returning the egg to the incubator. Once at the desired stage, embryos were isolated in cold 1X PBS and fixed overnight in 2% paraformaldehyde (PFA) at 4˚C, followed by PBS washes. Embryos were prepared for cryo-embedding by putting them through graded sucrose solutions ending in 30% sucrose overnight at 4˚C. Embryos were cryo-embedded in OCT (VWR 25608-930), sectioned to 15 µm, dried overnight, then stored at -80˚C.

Immunofluorescence (IF)

Cryosections were rehydrated in PBS then PBST (0.03% Tween-20), then blocked in 3% heat-inactivated goat serum (HIGS, Gibco 16210072) in PBST for 45 min at room temperature. Primary

antibodies were diluted in blocking solution (3% HIGS in PBST) and incubated either for 45 minutes at room temperature or overnight at 4˚C. After three PBST washes for five minutes each, secondary antibodies were incubated for 45 minutes at room temperature with 1:2000 dilution of DAPI added. PBST and PBS washes were done before mounting the slides with Prolong Gold anti-fade (Invitrogen P36930). Antigen retrieval pretreatment was necessary for GM130 (BD Biosciences 610822) immunofluorescent staining. Cryosections were rehydrated in water, then microwaved in 1:100 antigen-retrieval solution (Vector Laboratories, H-3300) until nearly boiling. After incubating at 37˚C wrapped in aluminum foil for 15 minutes and cooling for 10 minutes, slides were taken through the standard IHC protocol.

RNA *in situ* hybridization

Section and wholemount RNA *in situ* hybridization was done using a modified protocol from Moisés Mallo as previously described.[114]

Dextran injections

Dextran injections into the DM were done using 3000 MW dextran conjugated to fluorescein (ThermoFisher D3306) at a concentration of 10 mg/mL in 1X PBS with Fast Green dye added to better visualize the solution during injection. This mixture was loaded into fine pulled glass capillary needles. A microinjector with a foot pedal was set to 5 psi for 200 ms. Chicken embryos at the desired stage were prepared by removing the vitelline membrane. Injections were done to the right DM only, because embryos lie on their left sides from HH18 onwards and only the right DM is accessible for injection. With the anterior/posterior axis of the embryo perpendicular to the needle and with the needle at a 25˚ angle, the body wall was gently pulled back so the needle could access the right side of the DM. The needle was gently pressed into the tissue until the

embryo moved slightly from the force. Then the foot pedal was pressed once to inject. Embryos were allowed to continue incubating for about two hours, then embryos were collected and fixed in 2% PFA overnight at 4˚C. To screen for embryos with quality injections, embryos were cryo-embedded and sectioned. Any embryos with visible damage to the DM in these sections were excluded from further analysis.

AMD3100-BODIPY beading

AMD3100-BODIPY was synthesized as previously described,[61] and AG beads (Bio-Rad 143-1255) were soaked in 5 mg/ml AMD3100-BODIPY overnight nutating at 4°C. Drug-laden beads were inserted into the left coelomic cavity via a small incision, as previously described.[33]

CM-DiI and SP-DiO injections

Five µl of a stock solution of CM-DiI or SP-DiO (1µg/µl in EtOH) was diluted into 45 µl of prewarmed 0.3M sucrose in single distilled water maintained at 37˚C. Dye solutions were injected into the coelomic epithelium as previously described.[44]

Electroporation

DM electroporations were performed as described previously.[39,115] Endodermal electroporations were performed with a similar method, but with the electroporation mix (plasmid of interest and/or pCAG-GFP, 1X PBS, 1X Fast Green, 1mM MgCl2, and 0.17% carboxymethylcellulose) injected into the empty space beneath the ventral side of the embryo while the negative electrode was held in place there. The positive electrode was placed directly above the negative electrode, centered along the neural tube, before the pulse was applied. pCAGEN-Ntn4 expression plasmid was constructed by cloning the full-length coding sequence out of mouse Ntn4-AP-His plasmid (Addgene 71980) using the primers in Table 1, and cloning into pCAGEN (Addgene 11160) with

XhoI (NEB R0146) and NotI (NEB R0189). A second Ntn4 construct was also used, using a mouse Ntn4 (generously provided by Raphael Reuten) and cloned into the pMES vector,[116] with similar results.

Notochord transplants

Notochord transplants were performed on HH12-HH15 embryos, using a method adapted from papers describing notochordectomies and notochord transplants.[117–123] Note that notochordectomies, while potentially informative, were not done because damage to the endoderm is highly likely in those experiments. Since the endoderm is also potentially implicated in midline formation, an experiment that did not perturb that tissue was preferred. To prepare the donor notochord, the embryo was cut crosswise at the level of the vitelline arteries and close to the end of the tail. Clean 2-4 mm sections of notochord were used for the transplants. A sharp glass needle was used to make an incision in the recipient embryo along the anterior/posterior body axis between the neural tube and somites, deep enough so the ectopic notochord could sit next to the native notochord without puncturing the dorsal aorta. The donor notochord was pressed into place using a pair of dull glass needles or forceps. Embryos continued developing at 37˚C until stage HH19.

Scanning electron microscopy (SEM)

Embryos used for Fig. 3C and D were fixed in 4% paraformaldehyde and 2% glutaraldehyde in PBS overnight at 4˚C. Samples were then equilibrated in 5% sucrose/PBS for 1 hour at RT, 20% sucrose/PBS for 1 hour at RT, and finally 15% sucrose/7.5% gelatin/PBS at 37 degrees overnight. Embryos were then embedded in plastic molds and frozen in liquid Isopentane in a dry ice-ethanol bath. Cryosections of 10 microns in thickness were collected on poly-L-lysine treated coverslips

and incubated twice with fresh drops of PBS for 10 min at 37˚C. Coverslips were then washed with 0.1M cacodylate buffer and post fixed with 0.1% osmium tetroxide. Following washes with deuterium-depleted water (DDW), the sections were dehydrated in graded ethanol series, critical point dried (Quorum K850) and sputter coated with 6 nm of chromium (Quorum Q150T). Samples then were viewed on Zeiss Ultra Plus HR Scanning Electron Microscope using the SE2 detector.

Embryos for SEM in Fig. S1 were fixed in 2% glutaraldehyde in 0.50M cacodylate buffer (pH 7.4) at 4˚C for two hours, then rinsed three times for 10 minutes each in 0.05M cacodylate buffer. At this point, embryos were cut down to size, using sharp spring scissors to cut the embryo crosswise at the level of the midgut. Then embryos were post-fixed in 1% osmium tetroxide in 0.05M cacodylate buffer at 4˚C for one hour, rinsed again in 0.05M cacodylate buffer (3x 10 min), dehydrated in an ethanol series of 25%, 50%, 70%, 95%, and 100% for 10 minutes each, and left in 100% ethanol overnight. The following day embryos were critical point dried in CO_2, soaking for 24 hours. Samples were mounted and silver paint was used for conductivity. These embryos were sputter-coated with gold palladium and imaged on a LEO 1550 (Keck SEM).

Imaging, image processing, and quantifications

Brightfield and fluorescent images of tissue sections were taken on a Zeiss Observer Z1 with Apotome, a LSM880 Confocal multiphoton inverted microscope—i880 (Zeiss), or a LSM710 Confocal (Zeiss), or a ScanScope CS2. Stereoscopic images were taken on a SteREO Discovery.V12 (Zeiss). Images were processed using Fiji. Statistical analyses were done using GraphPad Prism.

Quantification of fluorescent intensity of laminin staining was done for five sum intensity projections per biological replicate. For each image, the width of the midline was averaged from three measurements. When no midline is discernible at HH21, the midline width for each image was replaced with the overall average HH20 midline width. Then, five profile plots of gray values

(intensity) were obtained from orthogonal lines drawn across the midline. The gray values within the average membrane width centered around the local maximum gray value were averaged to produce a raw mean midline gray value for each image. This process was repeated for neural floor plate basement membrane, and the raw mean midline gray value for each image was normalized to the raw mean floor plate basement membrane value. The means of HH18, HH19, HH20, and HH21 normalized midline gray values were compared via Welch's unequal variances t-test. Finally, midline length was measured at HH19 as the distance between the tip of the endoderm and the notochord from the hindgut (where the "bird's nest" of laminin deposition becomes longer than it is wide), to the cranial midgut (where the branches of the dorsal aorta fuse).

AMD3100-BODIPY diffusion was quantified by drawing an ROI across the DM bound by the dorsal aorta on top and the endoderm on the bottom. A profile plot of average gray values was obtained for each ROI for laminin and AMD3100-BODIPY separately. At HH19, the x-positions of laminin maxima corresponding to the left and right coelomic epithelium basement membrane and the midline basement membrane were used to divide the BODIPY intensity data into left and right DM compartments. At HH21 when no midline is present, left and right DM compartments were designated by dividing the distance between coelomic epithelial basement membranes in half. The separated left and right BODIPY data were then averaged to obtain a mean left DM and mean right DM BODIPY intensity value, which were compared to obtain the ratio of right versus left DM BODIPY signal. All intensity measurements were normalized for each image by subtracting the average gray value of the notochord in the 488 channel. These ratios were compared via Welch's unequal variances t-test.

GM130 Golgi staining was used to assess cell polarity as described previously.[38] Five cell populations were evaluated: cells contacting the midline on the left ("left margin"), cells contacting the midline on the right ("right margin"), right mesenchymal cells not contacting the

midline or coelomic epithelium, left coelomic epithelial cells, and rare cells observed between the double membrane of the midline itself ("midline cells") (Fig. 4D, Fig. S4). For each cell, the clockwise angle relative to vertical (0˚) of the line drawn between the center of the nucleus and the Golgi apparatus (Fig. 4D inset) was recorded and plotted on an angle histogram in 20° bins with five biological replicates each. The trend of cell polarity in each cell population was assessed using Rayleigh's test of uniformity using the "circular" R package for circular statistics (https://r-forge.r-project.org/projects/circular/).

Veiled chameleon husbandry, collection, and fixation

Veiled chameleon husbandry was performed at the Stowers Institute for Medical Research in the Reptiles and Aquatics Facility in accordance with the Institutional Animal Care and Use Committee approved protocol 2020-115, and as described previously.[124–126] following the protocols which are publicly available here: dx.doi.org/10.17504/protocols.io.bzhsp36e. Veiled chameleon eggs were collected at oviposition in the Reptiles and Aquatics Facility at Stowers Institute for Medical Research. Eggs were incubated in deli cups with moist vermiculite at a constant temperature of 28 ºC for 65-90 days to achieve desired staging. The eggs were cleared of large particles and wiped with RNaseZap wipes (Invitrogen AM9786) to minimize RNAse contamination. Clean eggs were candled to determine the position of the embryo under the leathery shell. We used fine scissors to cut a segment of the shell around the embryo and separate the embryo (attached to the shell) from the rest of the egg. The embryos were further separated from the shell and dissected out of the membranes in room temperature Tyrode's solution, made in DEPC-treated water. Subsequently the embryos were fixed overnight at 4 ºC in 4% PFA in DEPC 1X PBS, then dehydrated through an ascending methanol series into 100% methanol and stored at -20 ºC for future analysis. Stages of embryonic development were determined as previously described.[53]

Table 1. Reagents used in these experiments.

Reagent	Source	Catalog #	Sequence	Dilution
Anti-laminin alpha 1 (1˚ ab)	Sigma	L9393		1:100
Anti-laminin 1 (1˚ ab)	DSHB	3H11		1:10
Anti-perlecan (1˚ ab)	DSHB	5C9		1:10
Anti-nidogen (1˚ ab)	DSHB	1G12		1:10
Anti-fibronectin (1˚ ab)	DSHB	VA1(3)		1:5
Anti-fibronectin (1˚ ab)	DSHB	B3/D6		1:30
Anti-fibronectin (1˚ ab)	Sigma	F3648		1:400
Anti-GM130 (1˚ ab)	BD Biosciences	610822		1:250
Alexa Fluor 568 goat anti-rabbit (2˚ ab)	Invitrogen	A-11031		1:500
Alexa Fluor 647 donkey anti-rabbit (2˚ ab)	Invitrogen	A32795		1:500
Alexa Fluor 488 goat anti-mouse (2˚ ab)	Invitrogen	A32723		1:500
DAPI	Thermofisher	D1306		1:2000
Dextran, Fluorescein, 3000 MW, lysine fixable, anionic	Thermofisher	D3306		
CM-DiI	Invitrogen	C7000		
SP-DiO	Invitrogen	D7778		
Plasmid for chordin riboprobe (chicken)	Cliff Tabin lab	T691		
Plasmid for lefty1 riboprobe (chicken)	Cepko/Tabin lab	T607		
F primer for chicken LAMA1 riboprobe from cDNA			ACGGAGAGTTTGGCAGATGA	
R primer for chicken LAMA1 riboprobe from cDNA			ATCCTGAGCCCAAATCCCAA	
PCR cloning kit (pDrive plasmid)	Qiagen	231124		
pCAGEN	Connie Cepko	Addgene 11160		
pCAG-GFP	Connie Cepko	Addgene 11150		
pCI-H2B-RFP	Addgene	92398		
Ntn4-AP-His plasmid	Addgene	71980		
5' primer for cloning Ntn4 coding region out of Addgene 71980 and into pCAGEN (XhoI and NotI)			ATGCCTCGAGATATCgccaccatggggagctg	
3' primer for cloning Ntn4 coding region out of Addgene 71980 and into pCAGEN (XhoI and NotI)			CTAGCGGCCGCGGATCCATCGATTATTA CACGCAGTCTCTTTTTAAGATGTGCA	

Acknowledgements

We express deep gratitude to Drs. David Sherwood, Lydia Sorokin, Drew Noden, Gary Schoenwolf, and Peter Yurchenco for immensely helpful suggestions and wisdom. We deeply thank Dr. Ouathek Ouerfelli at Sloan Kettering for his services in synthesizing AMD3100-BODIPY. Sincere thanks go to Drs. John Grazul, Mariena Silvestry Ramos, and Shannon Caldwell (Cornell University), as well as Dr. Lihi Shaulov of the Technion Biomedical Electron Microscopy Center

for instruction and technical assistance with Scanning Electron Microscopy. We appreciate the Cornell Imaging Core (Drs. Rebecca Williams and Johanna Dela Cruz) for training and maintenance of the microscopes. Thanks to Rachel Slater-Buchanan, Brittany Laslow, and Erica Butler for technical support. We thank Dr. Raphael Reuten for providing mouse Netrin 4 plasmid. Gratitude goes to Dr. Shing Hu for helpful feedback on the manuscript. We acknowledge Dr. Aravind Sivakumar for Fig. 6A *Cxcl12* image and Dr. Bhargav Sanketi for Fig. 6B *BMP4* image. This work was supported by the following grants: National Institute of Diabetes and Digestive and Kidney Diseases (grants R01 DK092776 and R01 DK107634 to N.A.K.); the March of Dimes (grant 1-FY11-520 to N.A.K.); NSF GRFP (DGE -1650441 to C.D.); NIH S10RR025502 for data collected on the Zeiss LSM 710 Confocal, and NIH S10OD018516 for data collected on the inverted Zeiss LSM880 confocal/multiphoton microscope (i880); the Israel Science Foundation (grants 1463/16 and 1528/22 to T.M.S.); and the Israel Cancer Research Fund and the Rappaport Family Foundation to T.M.S.

References

1. McCain, E.R., and McClay, D.R. (1994). The establishment of bilateral asymmetry in sea urchin embryos. Development *120*. https://doi.org/10.1242/dev.120.2.395.
2. Danos, M.C., and Yost, H.J. (1995). Linkage of cardiac left-right asymmetry and dorsal-anterior development in Xenopus. Development *121*. https://doi.org/10.1242/dev.121.5.1467.
3. Levin, M., Johnson, R.L., Sterna, C.D., Kuehn, M., and Tabin, C. (1995). A molecular pathway determining left-right asymmetry in chick embryogenesis. Cell *82*. https://doi.org/10.1016/0092-8674(95)90477-8.
4. Nonaka, S., Tanaka, Y., Okada, Y., Takeda, S., Harada, A., Kanai, Y., Kido, M., and Hirokawa, N. (1998). Randomization of left-right asymmetry due to loss of nodal cilia generating leftward flow of extraembryonic fluid in mice lacking KIF3B motor protein. Cell *95*. https://doi.org/10.1016/S0092-8674(00)81705-5.
5. Nonaka, S., Shiratori, H., Saijoh, Y., and Hamada, H. (2002). Determination of left-right patterning of the mouse embryo by artificial nodal flow. Nature *418*. https://doi.org/10.1038/nature00849.
6. Essner, J.J., Amack, J.D., Nyholm, M.K., Harris, E.B., and Yost, H.J. (2005). Kupffer's vesicle is a ciliated organ of asymmetry in the zebrafish embryo that initiates left-right

development of the brain, heart and gut. Development *132*. https://doi.org/10.1242/dev.01663.

7. Schweickert, A., Weber, T., Beyer, T., Vick, P., Bogusch, S., Feistel, K., and Blum, M. (2007). Cilia-Driven Leftward Flow Determines Laterality in Xenopus. Current Biology *17*. https://doi.org/10.1016/j.cub.2006.10.067.
8. Gros, J., Feistel, K., Viebahn, C., Blum, M., and Tabin, C.J. (2009). Cell movements at Hensen's node establish left/right asymmetric gene expression in the chick. Science *324*, 941–944. https://doi.org/10.1126/science.1172478.
9. Maya-Ramos, L., and Mikawa, T. (2020). Programmed cell death along the midline axis patterns ipsilaterality in gastrulation. Science (1979) *367*. https://doi.org/10.1126/science.aaw2731.
10. Bisgrove, B.W., Essner, J.J., and Yost, H.J. (2000). Multiple pathways in the midline regulate concordant brain, heart and gut left-right asymmetry. Development *127*. https://doi.org/10.1242/dev.127.16.3567.
11. Yamamoto, M., Mine, N., Mochida, K., Sakai, Y., Saijoh, Y., Meno, C., and Hamada, H. (2003). Nodal signaling induces the midline barrier by activating Nodal expression in the lateral plate. Development *130*, 1795–1804. https://doi.org/10.1242/DEV.00408.
12. Meno, C., Saijoh, Y., Fujii, H., Ikeda, M., Yokoyama, T., Yokoyama, M., Toyoda, Y., and Hamada, H. (1996). Left-right asymmetric expression of the TGFβ-family member lefty in mouse embryos. Nature *381*. https://doi.org/10.1038/381151a0.
13. Meno, C., Shimono, A., Saijoh, Y., Yashiro, K., Mochida, K., Ohishi, S., Noji, S., Kondoh, H., and Hamada, H. (1998). lefty-1 Is Required for Left-Right Determination as a Regulator of lefty-2 and nodal. Cell *94*, 287–297. https://doi.org/10.1016/S0092-8674(00)81472-5.
14. Yoshioka, H., Meno, C., Koshiba, K., Sugihara, M., Itoh, H., Ishimaru, Y., Inoue, T., Ohuchi, H., Semina, E. V, Murray, J.C., et al. (1998). Pitx2, a Bicoid-Type Homeobox Gene, Is Involved in a Lefty-Signaling Pathway in Determination of Left-Right Asymmetry. Cell *94*, 299–305. https://doi.org/10.1016/S0092-8674(00)81473-7.
15. Bisgrove, B.W., Essner, J.J., and Yost, H.J. (1999). Regulation of midline development by antagonism of lefty and nodal signaling. Development *126*. https://doi.org/10.1242/dev.126.14.3253.
16. Kaufman, M.H. (2004). The embryology of conjoined twins. Child's Nervous System *20*. https://doi.org/10.1007/s00381-004-0985-4.
17. Levin, M., Roberts, D.J., Holmes, L.B., and Tabin, C. (1996). Laterality defects in conjoined twins. Nature *384*, 321–321. https://doi.org/10.1038/384321a0.
18. Tisler, M., Thumberger, T., Schneider, I., Schweickert, A., and Blum, M. (2017). Leftward Flow Determines Laterality in Conjoined Twins. Current Biology *27*. https://doi.org/10.1016/j.cub.2016.12.049.
19. Desgrange, A., Le Garrec, J.-F., and Meilhac, S.M. (2018). Left-right asymmetry in heart development and disease: forming the right loop. Development *145*, dev162776. https://doi.org/10.1242/dev.162776.
20. Duboc, V., Dufourcq, P., Blader, P., and Roussigné, M. (2015). Asymmetry of the Brain: Development and Implications. Annu Rev Genet *49*. https://doi.org/10.1146/annurev-genet-112414-055322.

21. Desgrange, A., Le Garrec, J.F., Bernheim, S., Bønnelykke, T.H., and Meilhac, S.M. (2020). Transient Nodal Signaling in Left Precursors Coordinates Opposed Asymmetries Shaping the Heart Loop. Dev Cell *55*. https://doi.org/10.1016/j.devcel.2020.10.008.
22. Cavalcante, L.A., Garcia-Abreu, J., Neto, V.M., Silva, L.C., and Weissmüller, G. (2002). Modulators of axonal growth and guidance at the brain midline with special reference to glial heparan sulfate proteoglycans. An Acad Bras Cienc *74*. https://doi.org/10.1590/S0001-37652002000400010.
23. Kullander, K., Croll, S.D., Zimmer, M., Pan, L., McClain, J., Hughes, V., Zabski, S., DeChiara, T.M., Klein, R., Yancopoulos, G.D., et al. (2001). Ephrin-B3 is the midline barrier that prevents corticospinal tract axons from recrossing, allowing for unilateral motor control. Genes Dev *15*. https://doi.org/10.1101/gad.868901.
24. Brose, K., Bland, K.S., Kuan, H.W., Arnott, D., Henzel, W., Goodman, C.S., Tessier-Lavigne, M., and Kidd, T. (1999). Slit proteins bind robo receptors and have an evolutionarily conserved role in repulsive axon guidance. Cell *96*. https://doi.org/10.1016/S0092-8674(00)80590-5.
25. Kidd, T., Brose, K., Mitchell, K.J., Fetter, R.D., Tessier-Lavigne, M., Goodman, C.S., and Tear, G. (1998). Roundabout controls axon crossing of the CNS midline and defines a novel subfamily of evolutionarily conserved guidance receptors. Cell *92*. https://doi.org/10.1016/S0092-8674(00)80915-0.
26. Erskine, L., Williams, S.E., Brose, K., Kidd, T., Rachel, R.A., Goodman, C.S., Tessier-Lavigne, M., and Mason, C.A. (2000). Retinal ganglion cell axon guidance in the mouse optic chiasm: Expression and function of Robos and Slits. Journal of Neuroscience *20*. https://doi.org/10.1523/jneurosci.20-13-04975.2000.
27. Neugebauer, J.M., and Joseph Yost, H. (2014). FGF signaling is required for brain left-right asymmetry and brain midline formation. Dev Biol *386*. https://doi.org/10.1016/j.ydbio.2013.11.020.
28. Katori, S., Noguchi-Katori, Y., Itohara, S., and Iwasato, T. (2017). Spinal racGAP α-chimaerin is required to establish the midline barrier for proper corticospinal axon guidance. Journal of Neuroscience *37*. https://doi.org/10.1523/JNEUROSCI.3123-16.2017.
29. Hounnou, G., Destrieux, C., Desmé, J., Bertrand, P., and Velut, S. (2002). Anatomical study of the length of the human intestine. Surgical and Radiologic Anatomy *24*. https://doi.org/10.1007/s00276-002-0057-y.
30. Stevens, C.E., and Hume, I.D. (1998). Contributions of microbes in vertebrate gastrointestinal tract to production and conservation of nutrients. Preprint, https://doi.org/10.1152/physrev.1998.78.2.393 https://doi.org/10.1152/physrev.1998.78.2.393.
31. Savin, T., Kurpios, N.A., Shyer, A.E., Florescu, P., Liang, H., Mahadevan, L., and Tabin, C.J. (2011). On the growth and form of the gut. Nature *476*, 57–62. https://doi.org/10.1038/nature10277.
32. Torres, A.M., and Ziegler, M.M. (1993). Malrotation of the intestine. World J Surg *17*. https://doi.org/10.1007/BF01658699.
33. Mahadevan, A., Welsh, I.C., Sivakumar, A., Gludish, D.W., Shilvock, A.R., Noden, D.M., Huss, D., Lansford, R., and Kurpios, N.A. (2014). The left-right Pitx2 pathway drives organ-specific arterial and lymphatic development in the intestine. Dev Cell *31*, 690–706. https://doi.org/10.1016/j.devcel.2014.11.002.

34. Hu, S., Mahadevan, A., Elysee, I.F., Choi, J., Souchet, N.R., Bae, G.H., Taboada, A.K., Sanketi, B., Duhamel, G.E., Sevier, C.S., et al. (2021). The asymmetric Pitx2 gene regulates gut muscular-lacteal development and protects against fatty liver disease. Cell Rep *37*. https://doi.org/10.1016/j.celrep.2021.110030.
35. Hecksher-Sørensen, J., Watson, R.P., Lettice, L.A., Serup, P., Eley, L., De Angelis, C., Ahlgren, U., and Hill, R.E. (2004). The splanchnic mesodermal plate directs spleen and pancreatic laterality, and is regulated by Bapx1/Nkx3.2. Development *131*. https://doi.org/10.1242/dev.01364.
36. Kurpios, N.A., Iban, M., Davis, N.M., Lui, W., Katz, T., and Martin, J.F. (2008). The direction of gut looping is established by changes in the extracellular matrix and in cell : cell adhesion. Proc Natl Acad Sci U S A *105*, 8499–8506.
37. Davis, N.M., Kurpios, N.A., Sun, X., Gros, J., Martin, J.F., and Tabin, C.J. (2008). The Chirality of Gut Rotation Derives from Left-Right Asymmetric Changes in the Architecture of the Dorsal Mesentery. Dev Cell *15*, 134–145. https://doi.org/10.1016/j.devcel.2008.05.001.
38. Welsh, I.C., Thomsen, M., Gludish, D.W., Alfonso-Parra, C., Bai, Y., Martin, J.F., and Kurpios, N.A. (2013). Integration of left-right Pitx2 transcription and Wnt signaling drives asymmetric gut morphogenesis via Daam2. Dev Cell *26*, 629–644. https://doi.org/10.1016/j.devcel.2013.07.019.
39. Sivakumar, A., Mahadevan, A., Lauer, M.E., Narvaez, R.J., Ramesh, S., Demler, C.M., Souchet, N.R., Hascall, V.C., Midura, R.J., Garantziotis, S., et al. (2018). Midgut Laterality Is Driven by Hyaluronan on the Right. Dev Cell *46*, 533-551.e5. https://doi.org/10.1016/j.devcel.2018.08.002.
40. Sanketi, B.D., Zuela-Sopilniak, N., Bundschuh, E., Gopal, S., Hu, S., Long, J., Lammerding, J., Hopyan, S., and Kurpios, N.A. (2022). Pitx2 patterns an accelerator-brake mechanical feedback through latent TGFβ to rotate the gut. Science (1979) *377*.
41. Hamburger, V., and Hamilton, H.L. (1951). A series of normal stages in the development of the chick embryo. J Morphol *88*, 49–92. https://doi.org/10.1002/jmor.1050880104.
42. Welsh, I.C., Kwak, H., Chen, F.L., Werner, M., Shopland, L.S., Danko, C.G., Lis, J.T., Zhang, M., Martin, J.F., and Kurpios, N.A. (2015). Chromatin Architecture of the Pitx2 Locus Requires CTCF- and Pitx2-Dependent Asymmetry that Mirrors Embryonic Gut Laterality. Cell Rep *13*, 337–349. https://doi.org/10.1016/j.celrep.2015.08.075.
43. Sivakumar, A., Mahadevan, A., Lauer, M.E., Narvaez, R.J., Ramesh, S., Demler, C.M., Souchet, N.R., Hascall, V.C., Midura, R.J., Garantziotis, S., et al. (2018). Midgut Laterality Is Driven by Hyaluronan on the Right. Dev Cell *46*. https://doi.org/10.1016/j.devcel.2018.08.002.
44. Arraf, A.A., Yelin, R., Reshef, I., Kispert, A., and Schultheiss, T.M. (2016). Establishment of the Visceral Embryonic Midline Is a Dynamic Process that Requires Bilaterally Symmetric BMP Signaling. Dev Cell *37*, 571–580. https://doi.org/10.1016/J.DEVCEL.2016.05.018.
45. Arraf, A.A., Yelin, R., Reshef, I., Jadon, J., Abboud, M., Zaher, M., Schneider, J., Vladimirov, F.K., and Schultheiss, T.M. (2020). Hedgehog Signaling Regulates Epithelial Morphogenesis to Position the Ventral Embryonic Midline. Dev Cell *53*. https://doi.org/10.1016/j.devcel.2020.04.016.

46. Yurchenco, P.D. (2011). Basement Membranes: Cell Scaffoldings and Signaling Platforms. Cold Spring Harb Perspect Biol *3*, a004911–a004911. https://doi.org/10.1101/cshperspect.a004911.
47. Bancroft, M., and Bellairs, R. (1976). The development of the notochord in the chick embryo, studied by scanning and transmission electron microscopy. J Embryol Exp Morphol *35*. https://doi.org/10.1242/dev.35.2.383.
48. Saraga Babić, M. (1990). Relationship between notochord and the bursa pharyngea in early human development. Cell Differentiation and Development *32*. https://doi.org/10.1016/0922-3371(90)90106-7.
49. Magro, G., and Grasso, S. (1995). Expression of cytokeratins, vimentin and basement membrane components in human fetal male Mullerian duct and perimullerian mesenchyme. Acta Histochem *97*. https://doi.org/10.1016/S0065-1281(11)80202-3.
50. Simon-Assmann, P., Lefebvre, O., Bellissent-Waydelich, A., Olsen, J., Orian-Rousseau, V., and De Arcangelis, A. (1998). The laminins: Role in intestinal morphogenesis and differentiation. In Annals of the New York Academy of Sciences https://doi.org/10.1111/j.1749-6632.1998.tb11110.x.
51. Horejs, C.M. (2016). Basement membrane fragments in the context of the epithelial-to-mesenchymal transition. Preprint, https://doi.org/10.1016/j.ejcb.2016.06.002 https://doi.org/10.1016/j.ejcb.2016.06.002.
52. Hu, Y.C., Okumura, L.M., and Page, D.C. (2013). Gata4 Is Required for Formation of the Genital Ridge in Mice. PLoS Genet *9*. https://doi.org/10.1371/journal.pgen.1003629.
53. Diaz, R.E., Shylo, N.A., Roellig, D., Bronner, M., and Trainor, P.A. (2019). Filling in the phylogenetic gaps: Induction, migration, and differentiation of neural crest cells in a squamate reptile, the veiled chameleon (Chamaeleo calyptratus). Developmental Dynamics *248*. https://doi.org/10.1002/dvdy.38.
54. Jayadev, R., and Sherwood, D.R. (2017). Basement membranes. Current Biology *27*, R199–R217.
55. Clark, R.A.F., Lanigan, J.M., DellaPelle, P., Manseau, E., Dvorak, H.F., and Colvin, R.B. (1982). Fibronectin and fibrin provide a provisional matrix for epidermal cell migration during wound reepithelialization. Journal of Investigative Dermatology *79*. https://doi.org/10.1111/1523-1747.ep12500075.
56. Glentis, A., Gurchenkov, V., and Vignjevic, D.M. (2014). Assembly, heterogeneity, and breaching of the basement membranes. Preprint, https://doi.org/10.4161/cam.28733 https://doi.org/10.4161/cam.28733.
57. Sasai, Y., Lu, B., Steinbeisser, H., Geissert, D., Gont, L.K., and De Robertis, E.M. (1994). Xenopus chordin: A novel dorsalizing factor activated by organizer-specific homeobox genes. Cell *79*. https://doi.org/10.1016/0092-8674(94)90068-X.
58. Streit, A., Lee, K.J., Woo, I., Roberts, C., Jessell, T.M., and Stern, C.D. (1998). Chordin regulates primitive streak development and the stability of induced neural cells, but is not sufficient for neural induction in the chick embryo. Development *125*. https://doi.org/10.1242/dev.125.3.507.
59. Schneiders, F.I., Maertens, B., Böse, K., Li, Y., Brunken, W.J., Paulsson, M., Smyth, N., and Koch, M. (2007). Binding of netrin-4 to laminin short arms regulates basement membrane assembly. Journal of Biological Chemistry *282*. https://doi.org/10.1074/jbc.M703137200.

60. Reuten, R., Patel, T.R., McDougall, M., Rama, N., Nikodemus, D., Gibert, B., Delcros, J.G., Prein, C., Meier, M., Metzger, S., et al. (2016). Structural decoding of netrin-4 reveals a regulatory function towards mature basement membranes. Nat Commun *7*. https://doi.org/10.1038/ncomms13515.
61. Poty, S., Désogère, P., Goze, C., Boschetti, F., D'huys, T., Schols, D., Cawthorne, C., Archibald, S.J., Maëcke, H.R., and Denat, F. (2015). New AMD3100 derivatives for CXCR4 chemokine receptor targeted molecular imaging studies: synthesis, anti-HIV-1 evaluation and binding affinities. Dalton Transactions *44*, 5004. https://doi.org/10.1039/c4dt02972k.
62. Carmona, R., Cano, E., Mattiotti, A., Gaztambide, J., and Muñoz-Chápuli, R. (2013). Cells Derived from the Coelomic Epithelium Contribute to Multiple Gastrointestinal Tissues in Mouse Embryos. PLoS One *8*. https://doi.org/10.1371/journal.pone.0055890.
63. Müller, P., Rogers, K.W., Yu, S.R., Brand, M., and Schier, A.F. (2013). Morphogen transport. Development (Cambridge) *140*. https://doi.org/10.1242/dev.083519.
64. Müller, P., and Schier, A.F. (2011). Extracellular Movement of Signaling Molecules. Preprint, https://doi.org/10.1016/j.devcel.2011.06.001 https://doi.org/10.1016/j.devcel.2011.06.001.
65. Bader, B.L., Smyth, N., Nedbal, S., Miosge, N., Baranowsky, A., Mokkapati, S., Murshed, M., and Nischt, R. (2005). Compound Genetic Ablation of Nidogen 1 and 2 Causes Basement Membrane Defects and Perinatal Lethality in Mice. Mol Cell Biol *25*. https://doi.org/10.1128/mcb.25.15.6846-6856.2005.
66. Miner, J.H. (2004). Compositional and structural requirements for laminin and basement membranes during mouse embryo implantation and gastrulation. Development *131*, 2247–2256. https://doi.org/10.1242/dev.01112.
67. Smyth, N., Vatansever, S.H., Murray, P., Meyer, M., Frie, C., Paulsson, M., and Edgar, D. (1999). Absence of basement membranes after targeting the LAMC1 gene results in embryonic lethality due to failure of endoderm differentiation. Journal of Cell Biology. https://doi.org/10.1083/jcb.144.1.151.
68. Gatseva, A., Sin, Y.Y., Brezzo, G., and Van Agtmael, T. (2019). Basement membrane collagens and disease mechanisms. Preprint, https://doi.org/10.1042/EBC20180071 https://doi.org/10.1042/EBC20180071.
69. Pozzi, A., Yurchenco, P.D., and Iozzo, R. V. (2017). The nature and biology of basement membranes. Preprint, https://doi.org/10.1016/j.matbio.2016.12.009 https://doi.org/10.1016/j.matbio.2016.12.009.
70. Yao, Y. (2017). Laminin: loss-of-function studies. Preprint, https://doi.org/10.1007/s00018-016-2381-0 https://doi.org/10.1007/s00018-016-2381-0.
71. Keeley, D.P., and Sherwood, D.R. (2019). Tissue linkage through adjoining basement membranes: The long and the short term of it. Preprint, https://doi.org/10.1016/j.matbio.2018.05.009 https://doi.org/10.1016/j.matbio.2018.05.009.
72. Pastor-Pareja, J.C. (2020). Atypical basement membranes and basement membrane diversity - What is normal anyway? Preprint, https://doi.org/10.1242/jcs.241794 https://doi.org/10.1242/jcs.241794.
73. Miner, J.H. (2012). The glomerular basement membrane. Exp Cell Res *318*, 973–978. https://doi.org/10.1016/j.yexcr.2012.02.031.

74. Naylor, R.W., Morais, M.R.P.T., and Lennon, R. (2021). Complexities of the glomerular basement membrane. Preprint, https://doi.org/10.1038/s41581-020-0329-y https://doi.org/10.1038/s41581-020-0329-y.
75. Daneman, R., and Prat, A. (2015). The blood–brain barrier. Cold Spring Harb Perspect Biol *7*. https://doi.org/10.1101/cshperspect.a020412.
76. Fausett, S.R., Brunet, L.J., and Klingensmith, J. (2014). BMP antagonism by noggin is required in presumptive notochord cells for mammalian foregut morphogenesis. Dev Biol *391*. https://doi.org/10.1016/j.ydbio.2014.02.008.
77. Jurand, A. (1974). Some aspects of the development of the notochord in mouse embryos. J Embryol Exp Morphol *32*. https://doi.org/10.1242/dev.32.1.1.
78. Trier, J.S., Allan, C.H., Abrahamson, D.R., and Hagen, S.J. (1990). Epithelial basement membrane of mouse jejunum. Evidence for laminin turnover along the entire crypt-villus axis. Journal of Clinical Investigation *86*. https://doi.org/10.1172/JCI114720.
79. Walser, M., Umbricht, C.A., Fröhli, E., Nanni, P., and Hajnal, A. (2017). β-Integrin de-phosphorylation by the Density-Enhanced Phosphatase DEP-1 attenuates EGFR signaling in C. elegans. PLoS Genet *13*. https://doi.org/10.1371/journal.pgen.1006592.
80. Naegeli, K.M., Hastie, E., Garde, A., Wang, Z., Keeley, D.P., Gordon, K.L., Pani, A.M., Kelley, L.C., Morrissey, M.A., Chi, Q., et al. (2017). Cell Invasion In Vivo via Rapid Exocytosis of a Transient Lysosome-Derived Membrane Domain. Dev Cell *43*. https://doi.org/10.1016/j.devcel.2017.10.024.
81. Matsuo, K., Koga, A., and Ihara, S. (2019). Visualization of endogenous NID-1 and EMB-9 in C. elegans. MicroPubl Biol.
82. Jayadev, R., Chi, Q., Keeley, D.P., Hastie, E.L., Kelley, L.C., and Sherwood, D.R. (2019). α-Integrins dictate distinct modes of type IV collagen recruitment to basement membranes. Journal of Cell Biology *218*. https://doi.org/10.1083/JCB.201903124.
83. Keeley, D.P., Hastie, E., Jayadev, R., Kelley, L.C., Chi, Q., Payne, S.G., Jeger, J.L., Hoffman, B.D., and Sherwood, D.R. (2020). Comprehensive Endogenous Tagging of Basement Membrane Components Reveals Dynamic Movement within the Matrix Scaffolding. Dev Cell *54*. https://doi.org/10.1016/j.devcel.2020.05.022.
84. Jayadev, R., Morais, M.R.P.T., Ellingford, J.M., Srinivasan, S., Naylor, R.W., Lawless, C., Li, A.S., Ingham, J.F., Hastie, E., Chi, Q., et al. (2022). A basement membrane discovery pipeline uncovers network complexity, regulators, and human disease associations. Sci Adv *8*. https://doi.org/10.1126/sciadv.abn2265.
85. Morin, X., Daneman, R., Zavortink, M., and Chia, W. (2001). A protein trap strategy to detect GFP-tagged proteins expressed from their endogenous loci in Drosophila. Proc Natl Acad Sci U S A *98*. https://doi.org/10.1073/pnas.261408198.
86. Ramos-Lewis, W., LaFever, K.S., and Page-McCaw, A. (2018). A scar-like lesion is apparent in basement membrane after wound repair in vivo. Matrix Biology *74*. https://doi.org/10.1016/j.matbio.2018.07.004.
87. Tomer, D., Arriagada, C., Munshi, S., Alexander, B.E., French, B., Vedula, P., Caorsi, V., House, A., Guvendiren, M., Kashina, A., et al. (2022). A new mechanism of fibronectin fibril assembly revealed by live imaging and super-resolution microscopy. J Cell Sci *135*. https://doi.org/10.1242/jcs.260120.
88. Morgner, J., Bornes, L., Hahn, K., Lopez-Iglesias, C., Kroese, L., Pritchard, C.E.J., Vennin, C., Peters, P.J., Huijbers, I., and van Rheenen, J. (2023). A Lamb1Dendra2 mouse

model identifies basement-membrane-producing origins and dynamics in PyMT breast tumors. Dev Cell *58*, 1–15.

89. Jain, P., Rauer, S.B., Möller, M., and Singh, S. (2022). Mimicking the Natural Basement Membrane for Advanced Tissue Engineering. Preprint, https://doi.org/10.1021/acs.biomac.2c00402 https://doi.org/10.1021/acs.biomac.2c00402.
90. Decaris, M.L., Gatmaitan, M., FlorCruz, S., Luo, F., Li, K., Holmes, W.E., Hellerstein, M.K., Turner, S.M., and Emson, C.L. (2014). Proteomic analysis of altered extracellular matrix turnover in bleomycin-induced pulmonary fibrosis. Molecular and Cellular Proteomics *13*. https://doi.org/10.1074/mcp.M113.037267.
91. Miyoshi, A., Kitajima, Y., Sumi, K., Sato, K., Hagiwara, A., Koga, Y., and Miyazaki, K. (2004). Snail and SIP1 increase cancer invasion by upregulating MMP family in hepatocellular carcinoma cells. Br J Cancer *90*. https://doi.org/10.1038/sj.bjc.6601685.
92. Miyoshi, A., Kitajima, Y., Kido, S., Shimonishi, T., Matsuyama, S., Kitahara, K., and Miyazaki, K. (2005). Snail accelerates cancer invasion by upregulating MMP expression and is associated with poor prognosis of hepatocellular carcinoma. Br J Cancer *92*. https://doi.org/10.1038/sj.bjc.6602266.
93. Sekiguchi, R., and Yamada, K.M. (2018). Basement Membranes in Development and Disease. In Current Topics in Developmental Biology https://doi.org/10.1016/bs.ctdb.2018.02.005.
94. Santiago-Medina, M., Gregus, K.A., Nichol, R.H., O'Toole, S.M., and Gomez, T.M. (2015). Regulation of ECM degradation and axon guidance by growth cone invadosomes. J Cell Sci *128*. https://doi.org/10.1242/jcs.169201.
95. Dickinson, A.J.G., and Sive, H. (2006). Development of the primary mouth in Xenopus laevis. Dev Biol *295*. https://doi.org/10.1016/j.ydbio.2006.03.054.
96. Hakanen, J., and Salminen, M. (2015). Defects in neural guidepost structures and failure to remove leptomeningeal cells from the septal midline behind the interhemispheric fusion defects in Netrin1 deficient mice. International Journal of Developmental Neuroscience *47*. https://doi.org/10.1016/j.ijdevneu.2015.08.005.
97. Gobius, I., Morcom, L., Suárez, R., Bunt, J., Bukshpun, P., Reardon, W., Dobyns, W.B., Rubenstein, J.L.R., Barkovich, A.J., Sherr, E.H., et al. (2016). Astroglial-Mediated Remodeling of the Interhemispheric Midline Is Required for the Formation of the Corpus Callosum. Cell Rep *17*. https://doi.org/10.1016/j.celrep.2016.09.033.
98. Torres, M., Gómez-Pardo, E., and Gruss, P. (1996). Pax2 contributes to inner ear patterning and optic nerve trajectory. Development *122*. https://doi.org/10.1242/dev.122.11.3381.
99. Barbieri, A.M., Broccoli, V., Bovolenta, P., Alfano, G., Marchitiello, A., Mocchetti, C., Crippa, L., Bulfone, A., Marigo, V., Ballabio, A., et al. (2002). Vax2 inactivation in mouse determines alteration of the eye dorsal-ventral axis, misrouting of the optic fibres and eye coloboma. Development *129*. https://doi.org/10.1242/dev.129.3.805.
100. Patel, A., and Sowden, J.C. (2019). Genes and pathways in optic fissure closure. Preprint, https://doi.org/10.1016/j.semcdb.2017.10.010 https://doi.org/10.1016/j.semcdb.2017.10.010.
101. ALSomiry, A.S., Gregory-Evans, C.Y., and Gregory-Evans, K. (2019). An update on the genetics of ocular coloboma. Hum Genet *138*. https://doi.org/10.1007/s00439-019-02019-3.

102. Lohr, J.L., Danos, M.C., and Yost, H.J. (1997). Left-right asymmetry of a nodal-related gene is regulated by dorsoanterior midline structures during Xenopus development. Development *124*, 1465–1472.
103. Chen, J.N., van Eeden, F.J., Warren, K.S., Chin, A., Nüsslein-Volhard, C., Haffter, P., and Fishman, M.C. (1997). Left-right pattern of cardiac BMP4 may drive asymmetry of the heart in zebrafish. Development.
104. James, R.G., and Schultheiss, T.M. (2003). Patterning of the avian intermediate mesoderm by lateral plate and axial tissues. Dev Biol *253*. https://doi.org/10.1006/dbio.2002.0863.
105. Natsis, K., Piagkou, M., Skotsimara, A., Protogerou, V., Tsitouridis, I., and Skandalakis, P. (2014). Horseshoe kidney: A review of anatomy and pathology. Preprint, https://doi.org/10.1007/s00276-013-1229-7 https://doi.org/10.1007/s00276-013-1229-7.
106. Tripathi, P., Guo, Q., Wang, Y., Coussens, M., Liapis, H., Jain, S., Kuehn, M.R., Capecchi, M.R., and Chen, F. (2010). Midline signaling regulates kidney positioning but not nephrogenesis through Shh. Dev Biol *340*. https://doi.org/10.1016/j.ydbio.2010.02.007.
107. Garriock, R.J., Czeisler, C., Ishii, Y., Navetta, A.M., and Mikawa, T. (2010). An anteroposterior wave of vascular inhibitor downregulation signals aortae fusion along the embryonic midline axis. Development *137*. https://doi.org/10.1242/dev.051664.
108. Jadon, J., Yelin, R., Arraf, A.A., Asleh, M.A., Zaher, M., and Schultheiss, T.M. (2023). Regulation of Aortic Morphogenesis and VE-Cadherin Dynamics by VEGF. Dev Biol *497*, 1–10.
109. Vokes, S.A., Yatskievych, T.A., Heimark, R.L., McMahon, J., McMahon, A.P., Antin, P.B., and Krieg, P.A. (2004). Hedgehog signaling is essential for endothelial tube formation during vasculogenesis. Development *131*. https://doi.org/10.1242/dev.01304.
110. Reese, D.E., Hall, C.E., and Mikawa, T. (2004). Negative regulation of midline vascular development by the notochord. Dev Cell *6*. https://doi.org/10.1016/S1534-5807(04)00127-3.
111. Sato, Y. (2013). Dorsal aorta formation: Separate origins, lateral-to-medial migration, and remodeling. Preprint, https://doi.org/10.1111/dgd.12010 https://doi.org/10.1111/dgd.12010.
112. Li, Y., Litingtung, Y., Ten Dijke, P., and Chiang, C. (2007). Aberrant Bmp signaling and notochord delamination in the pathogenesis of esophageal atresia. Developmental Dynamics *236*. https://doi.org/10.1002/dvdy.21075.
113. Hajduk, P., May, A., Puri, P., and Murphy, P. (2012). The Effect of Adriamycin Exposure on the Notochord of Mouse Embryos. Birth Defects Res B Dev Reprod Toxicol *95*. https://doi.org/10.1002/bdrb.21002.
114. Aires, R., de Lemos, L., Nóvoa, A., Jurberg, A.D., Mascrez, B., Duboule, D., and Mallo, M. (2019). Tail Bud Progenitor Activity Relies on a Network Comprising Gdf11, Lin28, and Hox13 Genes. Dev Cell *48*. https://doi.org/10.1016/j.devcel.2018.12.004.
115. Sanketi, B.D., and Kurpios, N.A. (2022). In Ovo Gain- and Loss-of-Function Approaches to Study Gut Morphogenesis. In Methods in Molecular Biology https://doi.org/10.1007/978-1-0716-2035-9_11.
116. Swartz, M.E., Eberhart, J., Pasquale, E.B., and Krull, C.E. (2001). EphA4/ephrin-A5 interactions in muscle precursor cell migration in the avian forelimb. Development *128*. https://doi.org/10.1242/dev.128.23.4669.

117. Teillet, M.A., and Le Douarin, N.M. (1983). Consequences of neural tube and notochord excision on the development of the peripheral nervous system in the chick embryo. Dev Biol. https://doi.org/10.1016/0012-1606(83)90349-4.
118. Klessinger, S., and Christ, B. (1996). Axial structures control laterality in the distribution pattern of endothelial cells. Anat Embryol (Berl) *193*, 319–330. https://doi.org/10.1007/BF00186689.
119. Artinger, K.B., and Bronner-Fraser, M. (1993). Delayed formation of the floor plate after ablation of the avian notochord. Neuron *11*, 1147–1161. https://doi.org/10.1016/0896-6273(93)90227-I.
120. van Straaten, H.W.M., Hekking, J.W.M., Thors, F., Wiertz-Hoessels, E.L., and Drukker, J. (1985). Induction of an additional floor plate in the neural tube. Acta Morphol Neerl Scand *23*.
121. van Straaten, H.W.M., Hekking, J.W.M., Wiertz-Hoessels, E.J.L.M., Thors, F., and Drukker, J. (1988). Effect of the notochord on the differentiation of a floor plate area in the neural tube of the chick embryo. Anat Embryol (Berl) *177*. https://doi.org/10.1007/BF00315839.
122. Yamada, T., Placzek, M., Tanaka, H., Dodd, J., and Jessell, T.M. (1991). Control of cell pattern in the developing nervous system: Polarizing activity of the floor plate and notochord. Cell *64*. https://doi.org/10.1016/0092-8674(91)90247-V.
123. Pettway, Z., Guillory, G., and Bronner-Fraser, M. (1990). Absence of neural crest cells from the region surrounding implanted notochordsin situ. Dev Biol *142*. https://doi.org/10.1016/0012-1606(90)90354-L.
124. Diaz, R.E., Anderson, C. V., Baumann, D.P., Kupronis, R., Jewell, D., Piraquive, C., Kupronis, J., Winter, K., Greek, T.J., and Trainor, P.A. (2015). Captive care, raising, and breeding of the veiled chameleon (Chamaeleo calyptratus). Cold Spring Harb Protoc *2015*. https://doi.org/10.1101/pdb.prot087718.
125. Diaz, R.E., Anderson, C. V., Baumann, D.P., Kupronis, R., Jewell, D., Piraquive, C., Kupronis, J., Winter, K., Bertocchini, F., and Trainor, P.A. (2015). The veiled chameleon (Chamaeleo calyptratus Duméril and Duméril 1851): A model for studying reptile body plan development and evolution. Cold Spring Harb Protoc *2015*. https://doi.org/10.1101/pdb.emo087700.
126. Diaz, R.E., Bertocchini, F., and Trainor, P.A. (2017). Lifting the veil on reptile embryology: The veiled chameleon (Chamaeleo calyptratus) as a model system to study reptilian development. In Methods in Molecular Biology https://doi.org/10.1007/978-1-4939-7216-6_18.

FIGURE LEGENDS

Figure 1. LR asymmetry in the DM is critical for proper gut looping and vascular patterning. (A) Asymmetries in the DM drive the formation of the first and subsequent gut loops. Concurrently, the vasculature is being patterned in the DM. The 1˚ longitudinal artery (*) gives rise to the ileocolic artery, which provides a significant portion of the adult intestine with critical blood flow. **(B)** HH17: The DM has cellular symmetry. HH18 and 19: The right mesenchyme begins expanding and the right epithelial cells elongate. The right-sided endothelial cells (vascular precursors) begin to disperse and leave the compartment, while the left-sided endothelium is maintained to become the future gut arteries. HH22: The asymmetric forces have pushed the gut tube to the left. A left-sided blood vessel, the 1˚ longitudinal artery (*) has formed. GT = gut tube, DM = dorsal mesentery, DA = dorsal aorta, SMA = superior mesenteric artery.

Figure 2. During DM formation from EMT and ingression of the coelomic epithelia, right and left cells do not mix. When the coelomic cavity is injected with DiI at HH12-13, n = 5 **(A)**, the labeled cells give rise to the mesenchymal and epithelial cells of the DM on the corresponding side of the embryo, n = 5 **(B)**. When DiI and DiO are injected at HH12-13 into left and right coeloms, respectively, n = 6 **(C)**, labeled cells are still segregated at HH18, n = 6 **(D, E and F)**. The same results are found when cells are labeled by electroporation with pCAG-GFP (left) and pCI-H2B-RFP (right) **(G and H),** both when the midline is continuous (HH19 n = 3, **G**) and once it has disappeared (HH21 n = 3, **H**). **(I-L)** H&E staining of the DM at HH18 n = 5 **(I)** shows "empty space" between the notochord, endoderm, and dorsal aortae. At HH19 n = 5 **(J)**, this space gains some cells (arrows), and the space is completely filled in by HH20 n = 4 **(K)**, and HH21 n = 3 **(L)**. Scale bars = 60 µm. nt = neural tube, c = coelom, ao = aorta, N = notochord, s = somite, DM = dorsal mesentery, L = left, R = right.

Figure 3. The DM midline is marked by laminin immunofluorescence. (A) *Lefty1* expression is seen at the embryonic midline of this HH9 embryo n = 4 (arrow). **(B)** *Lefty1* expression is not seen at the midline of the DM (dashed box) of an HH19 embryo (n=4). (Notochord=positive control.) **(C, D)** Scanning electron microscopy (SEM) images of a fixed embryo at HH15-16 show fibrous ECM between the notochord and endoderm. C is from a more posterior axial level than D. **(E-H)** Time course of midline dynamics from HH18-HH21, marked by laminin. Scale bars = 25 µm. **(I)** Quantification of the intensity of laminin immunofluorescence over development, normalized to laminin staining around the neural tube. Biological replicates: HH18 n = 2, HH19 n = 3, HH20 n = 3, and HH21 n = 2. Each dot represents one image quantified. Statistical analyses are unpaired Welch's t-tests. HH18-19: $p = 0.0188$, HH19-20: $p = 0.0118$, HH20-21: $p = 0.0003$. Additionally, there is a significant ($p < 0.0001$) linear trend among the means from HH18 to HH21 with a slope of -0.1019, $r^2 = 0.5906$. **(J)** Midline appearance from hindgut to foregut in an HH19 embryo, marked by laminin. Scale bars = 25 µm. **(K)** Quantification of DM midline length (dashed line) of three HH19 embryos, from the separation of the notochord and endoderm (hindgut) to the fusion of the aortae (foregut, coinciding with midline fragmentation). **(L)** Model of DM midline time kinetics. N = notochord, E/en = endoderm, Ao = aorta, nt = neural tube, c = coelomic cavity, CE = coelomic epithelium, L = left, R = right.

Figure 4. The midline basement membrane is not made by the DM mesenchyme or EMT of the endoderm, and the notochord is not sufficient for midline formation. (A-C) *Lama1* RNA *in situ* hybridization and adjacent sections with laminin IF staining at HH16 n = 3, HH18 n = 9, and HH19 n = 10 **(A'-C')**. Scale bars = 50 µm. **(D, E)** Cell polarity analysis from GM130 staining

shows that the mesenchymal cells immediately to the left or right of the midline ("left/right margin") and within the double membrane ("midline cells" have random polarity, as do the cells of the right mesenchyme (random polarization control); in contrast to the strong apical-basal polarity in cells of the left coelomic epithelium. Five embryos were used for these quantifications. Number of cells per circle histogram: left coelomic epithelium = 209, left margin = 346, midline cells = 118, right margin = 413, right mesenchyme = 514, right coelomic epithelium = 295. **(F)** Electroporation mix containing pCAGEN-GFP plasmid was injected under an HH14/15 embryo and then electroporated to specifically target the endoderm. Lineage tracing endoderm-derived cells to HH19 n = 8 **(G)** and HH21 n = 2 **(H)** by pCAGEN-GFP electroporation of the endoderm. **(I)** Model of notochord transplant method. A piece of notochord (red) was isolated from an HH14 donor embryo. In a stage-matched recipient, a cut was made adjacent to the neural tube and the donor notochord was inserted into this slit. **(J, L)** RNA *in situ* hybridization for Chordin to mark the native notochord (blue dashed circle) and transplanted notochord (red dashed circle). **(K, M)** Laminin immunohistochemistry to mark basement membrane including the midline (white arrow). Notochords are marked with an N (native notochord) and N* (transplanted notochord). **(J)** and **(K)** are from the same embryo, as are **(L)** and **(M)**. n = 8, scale bars = 50 µm. GT = gut tube, DM = dorsal mesentery, E = endoderm.

Figure 5. Ectopic expression of Netrinn4 by electroporation visibly affects the basement membrane underlying the coelomic epithelium, but not that underlying the endoderm, or the midline. (A, C) Electroporation of the left **(A)** or right **(C)** DM with the control, pCAG-GFP, had no effect on the basement membrane of the coelomic epithelium (arrows). Left n = 6. Right n = 4. **(B, D)** Electroporation of mouse Netrin4 (pCAGEN-Ntn4) and pCAG-GFP into the left **(B)** or right **(D)** DM disrupted the basement membrane underlying the coelomic epithelium (arrows) and scattered basement membrane in the mesenchyme (asterisks). Left n = 5. Right n = 5. The intact laminin staining in **B** is the basement membrane (BM) of the nephric duct. **(E)** Double DM electroporations also disrupt the coelomic epithelium (arrows) but the midline appears intact despite being contacted by Ntn4+ cells (n = 3). **(F, G)** Electroporation of the endoderm directly with pCAG-GFP or pCAGEN-Ntn4 does not visibly affect the basement membrane underlying the endoderm (open round pointers). Control n = 5. Ntn4 n = 8. The midline appears unaffected by any of these perturbations. Scale bars = 100 µm.

Figure 6. The DM midline serves as a barrier against diffusion. (A, B) Genes encoding diffusible signals including *Cxcl12* and *Bmp4* are expressed asymmetrically in the DM at HH19. **(C)** Hypothesis for the role of the midline in limiting diffusion of left and right signals across DM. **(D)** At HH19, the midline is intact (white arrow) and diffusion of 3000 MW dextran (green) is limited to the right side (n = 4/4). **(E)** At HH20, the midline (white arrow) has begun to fragment. Diffusion across the midline is prohibited in some embryos (n = 2/9) but permitted in others (n = 7/9). **(F)** At later stages when the midline has disappeared, diffusion is allowed through the DM (n = 7/7). **(G)** Proportion of dextran-labeled cells in the left vs. right DM, with unpaired t test. **(H)** At HH19, the midline is intact and diffusion of AMD3100-BODIPY is limited to the left side (n = 4). Dashed yellow box indicates quantified area. **(I)** At HH21 when the midline has disappeared, diffusion is allowed through the DM (n = 3). Dashed yellow box indicates quantified area. **(J)** Proportion of BODIPY intensity in the right vs. left DM, with unpaired t test. Each dot represents one image quantified. **(K, L)** Profile plot of average BODIPY intensity across the DM within the dashed yellow boxes in H and I, with left and right compartments of the DM overlayed. **(M)** Schematic of dextran injections into the right DM and AMD3100-BODIPY beading into the left DM. Scale bars = 50

um. LDM = left dorsal mesentery. RDM = right dorsal mesentery. GT = gut tube. E = endoderm. L = left. R = right. N = notochord. DA = dorsal aorta.

Figure 7. Model of endoderm descending hypothesis for midline formation. We hypothesize that as the endoderm moves ventrally and the distance between the notochord and endoderm grows, basement membrane from the endoderm may be left behind. This can be compared to a zipper where each side is the basement membrane underlying the endoderm, and when the zipper pull (tip of endoderm) moves downwards, the basement membrane behind it pulls closer together.

Supplemental Figure 1. SEM of cross-sections of chicken embryos at different stages of midline development. HH15 n = 2, HH17 n = 2, HH18 n = 3, HH19 n = 3. Yellow boxes indicate position of higher magnification images on right.

Supplemental Figure 2. Pseudotime kinetics of the midline along the anterior-posterior axis. (A-D) Laminin (green) and fibronectin (red) highlight the midline and aorta/e, respectively, in this HH17 embryo. The maturation of the midline occurs in an anterior-to-posterior wave (from **A** to **D**), as does the fusing of the two branches of the aorta into one (**A-D**, asterisks). Immunohistochemistry images were taken at approximately the axial level shown in the above cartoon (cartoons not to scale). Notice that the midline at a more anterior position in a younger HH12-13 **(E-H)** embryo appears similar to the midline at a more posterior position in an older embryo. Scale bars = 100 µm.

Supplemental Figure 3. The required basement membrane components nidogen and perlecan co-localize with laminin at the midline. (A) Nidogen co-localizes with laminin at the midline n = 4. **(B)** Perlecan co-localizes with laminin at the midline n = 4. **(C)** Fibronectin surrounds the dorsal aortae and is only found in the midline nearest the endoderm n = 6. Scale bars = 25 µm.

Supplemental Figure 4. GM130 staining for polarity analysis. (A, B) Example of GM130 staining at HH19 used for cell polarity analysis in Fig. 4, with key. **(B')** Dotted region of interest in B is magnified. Five embryos were used for these quantifications. Scale bars = 50 µm. CE = coelomic epithelium, DA = dorsal aorta, E = endoderm, N = notochord.

Supplemental Figure 5. The midline is conserved in a squamate and follows a similar trajectory of degradation. (A-C) Stages 24-25 n = 10; 26-28 n = 9 of veiled chameleon embryos, *Chamaeleo calyptratus* by somite stage as shown in Diaz et al. 2019.[53] Scale bars = 50 µm. GT = gut tube, DM = dorsal mesentery, E = endoderm, DA = dorsal aorta.

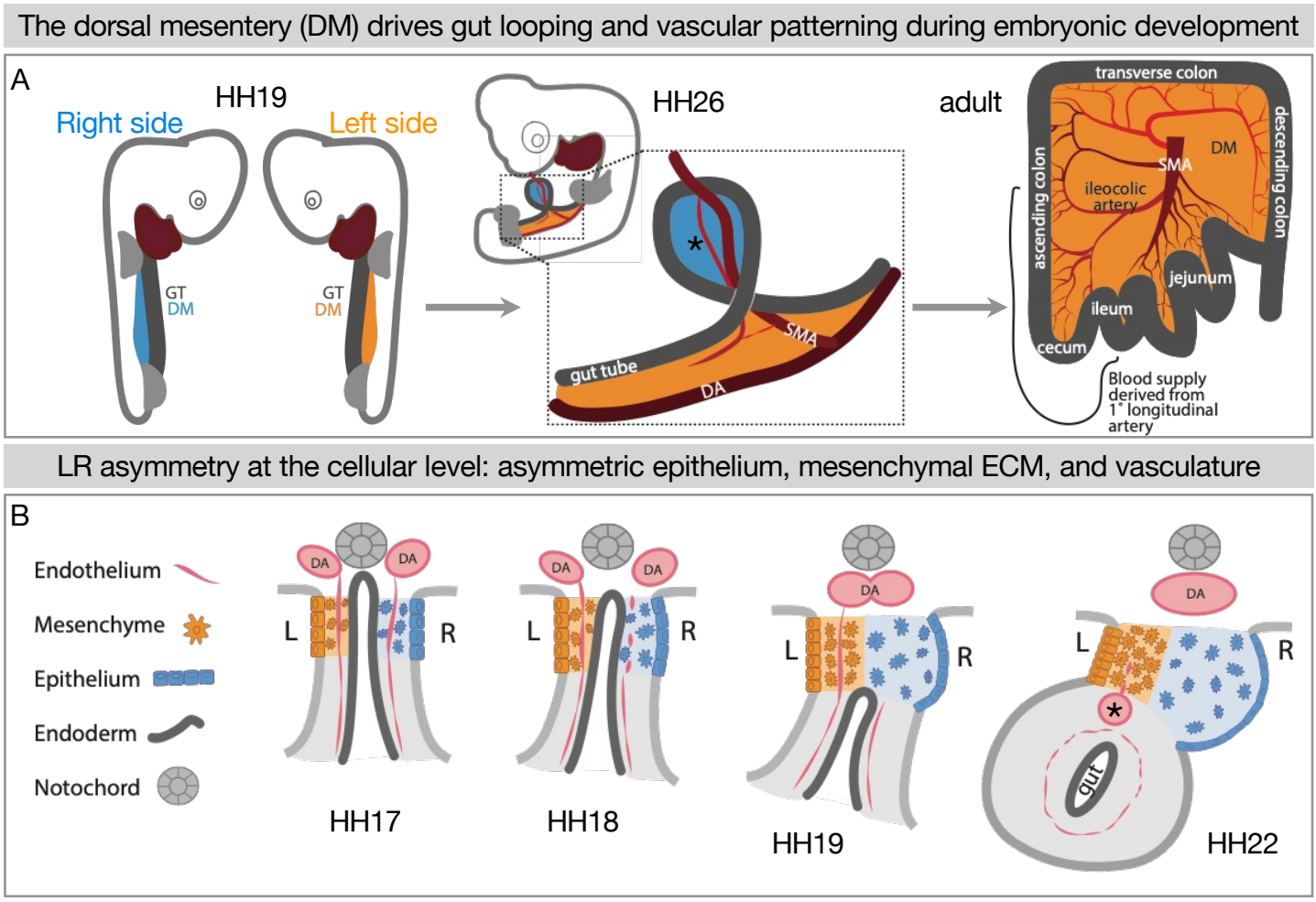
The dorsal mesentery (DM) drives gut looping and vascular patterning during embryonic development
A
HH19
Right side
Left side
GT
DM
GT
DM
HH26
gut tube
SMA
DA
adult
transverse colon
descending colon
ascending colon
DM
SMA
ileocolic artery
jejunum
ileum
cecum
Blood supply derived from 1° longitudinal artery
LR asymmetry at the cellular level: asymmetric epithelium, mesenchymal ECM, and vasculature
B
Endothelium
Mesenchyme
Epithelium
Endoderm
Notochord
DA
L
R
HH17
HH18
HH19
HH22
gut

FIGURE 1

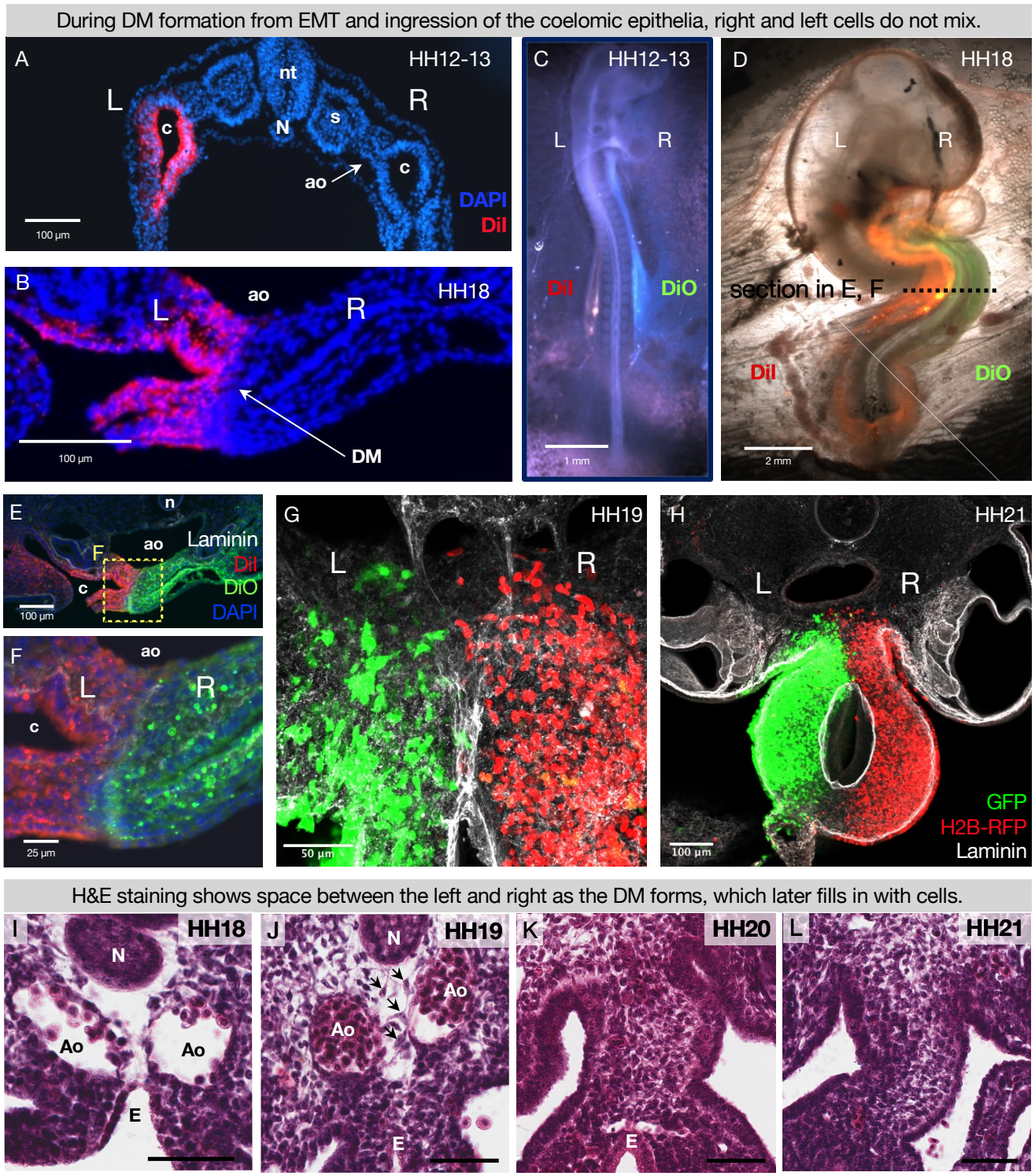
During DM formation from EMT and ingression of the coelomic epithelia, right and left cells do not mix.
A
HH12-13
nt
L
R
c
N
s
ao
c
DAPI
DiI
100 µm
B
HH18
L
ao
R
DM
100 µm
C
HH12-13
L
R
DiI
DiO
1 mm
D
HH18
L
R
section in E, F
DiI
DiO
2 mm
E
n
ao
Laminin
F
DiI
c
DiO
DAPI
100 µm
F
ao
L
R
c
25 µm
G
HH19
L
R
50 µm
H
HH21
L
R
GFP
H2B-RFP
Laminin
100 µm
H&E staining shows space between the left and right as the DM forms, which later fills in with cells.
I
HH18
N
Ao
Ao
E
J
HH19
N
Ao
Ao
E
K
HH20
E
L
HH21

FIGURE 2

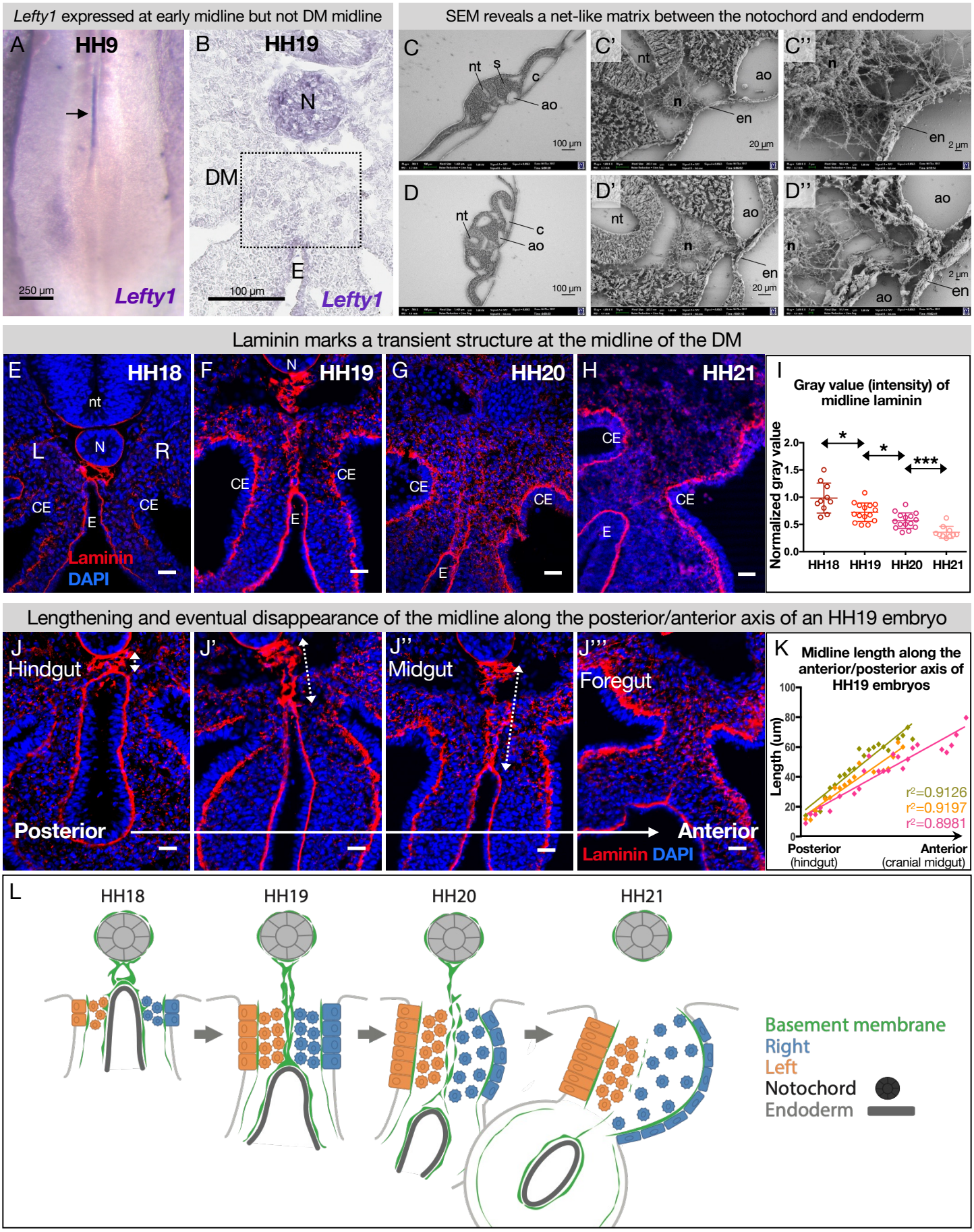
Lefty1 expressed at early midline but not DM midline
A
HH9
250 µm
Lefty1
B
HH19
N
DM
E
100 µm
Lefty1
SEM reveals a net-like matrix between the notochord and endoderm
C
nt
s
c
ao
100 µm
C'
nt
ao
n
en
20 µm
C''
n
en
2 µm
D
nt
c
ao
100 µm
D'
nt
ao
n
en
20 µm
D''
ao
n
2 µm
en
ao
Laminin marks a transient structure at the midline of the DM
E
HH18
nt
L
N
R
CE
CE
E
Laminin
DAPI
F
N
HH19
CE
CE
E
G
HH20
CE
CE
E
H
HH21
CE
CE
E
I
Gray value (intensity) of midline laminin
Normalized gray value
2.0
1.5
1.0
0.5
0.0
*
*
***
HH18
HH19
HH20
HH21
Lengthening and eventual disappearance of the midline along the posterior/anterior axis of an HH19 embryo
J
Hindgut
Posterior
J'
J''
Midgut
J'''
Foregut
Anterior
Laminin DAPI
K
Midline length along the anterior/posterior axis of HH19 embryos
Length (um)
100
80
60
40
20
0
r²=0.9126
r²=0.9197
r²=0.8981
Posterior
(hindgut)
Anterior
(cranial midgut)
L
HH18
HH19
HH20
HH21
Basement membrane
Right
Left
Notochord
Endoderm

FIGURE 3

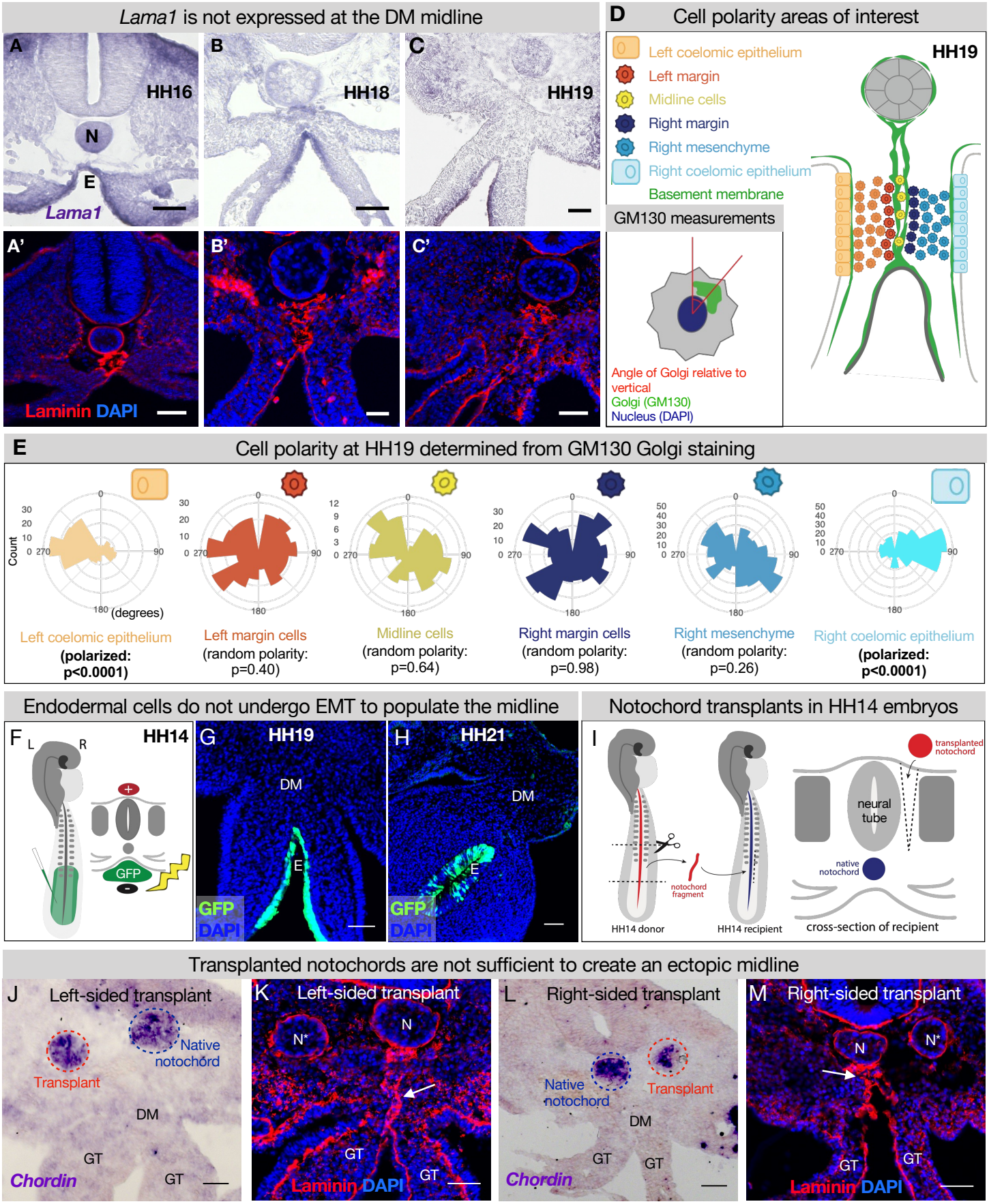
Lama1 is not expressed at the DM midline
A
HH16
N
E
Lama1
B
HH18
C
HH19
A'
B'
C'
Laminin DAPI
D
Cell polarity areas of interest
Left coelomic epithelium
Left margin
Midline cells
Right margin
Right mesenchyme
Right coelomic epithelium
Basement membrane
HH19
GM130 measurements
Angle of Golgi relative to vertical
Golgi (GM130)
Nucleus (DAPI)
E
Cell polarity at HH19 determined from GM130 Golgi staining
Count
(degrees)
Left coelomic epithelium
(polarized: p<0.0001)
Left margin cells
(random polarity: p=0.40)
Midline cells
(random polarity: p=0.64)
Right margin cells
(random polarity: p=0.98)
Right mesenchyme
(random polarity: p=0.26)
Right coelomic epithelium
(polarized: p<0.0001)
Endodermal cells do not undergo EMT to populate the midline
F
L
R
HH14
GFP
G
HH19
DM
E
GFP
DAPI
H
HH21
DM
E
GFP
DAPI
Notochord transplants in HH14 embryos
I
notochord fragment
HH14 donor
HH14 recipient
transplanted notochord
neural tube
native notochord
cross-section of recipient
Transplanted notochords are not sufficient to create an ectopic midline
J
Left-sided transplant
Native notochord
Transplant
DM
GT
GT
Chordin
K
Left-sided transplant
N
N*
GT
GT
Laminin DAPI
L
Right-sided transplant
Native notochord
Transplant
DM
GT
GT
Chordin
M
Right-sided transplant
N
N*
GT
GT
Laminin DAPI

FIGURE 4

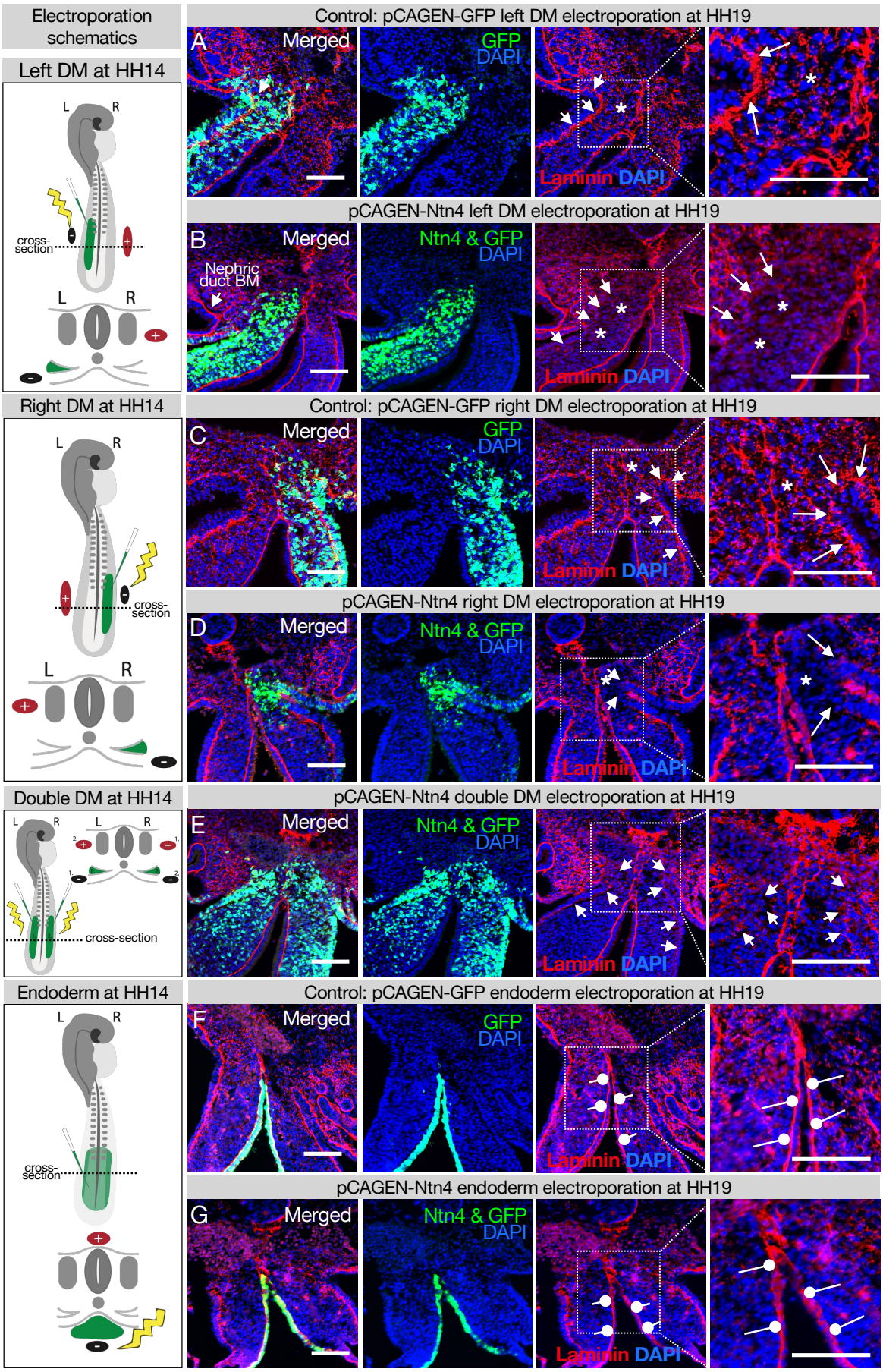
Electroporation schematics
Left DM at HH14
Right DM at HH14
Double DM at HH14
Endoderm at HH14
L
R
cross-section
Control: pCAGEN-GFP left DM electroporation at HH19
pCAGEN-Ntn4 left DM electroporation at HH19
Control: pCAGEN-GFP right DM electroporation at HH19
pCAGEN-Ntn4 right DM electroporation at HH19
pCAGEN-Ntn4 double DM electroporation at HH19
Control: pCAGEN-GFP endoderm electroporation at HH19
pCAGEN-Ntn4 endoderm electroporation at HH19
A
B
C
D
E
F
G
Merged
GFP
DAPI
Ntn4 & GFP
Laminin
Nephric duct BM

FIGURE 5

Diffusible signals are expressed asymmetrically in the DM

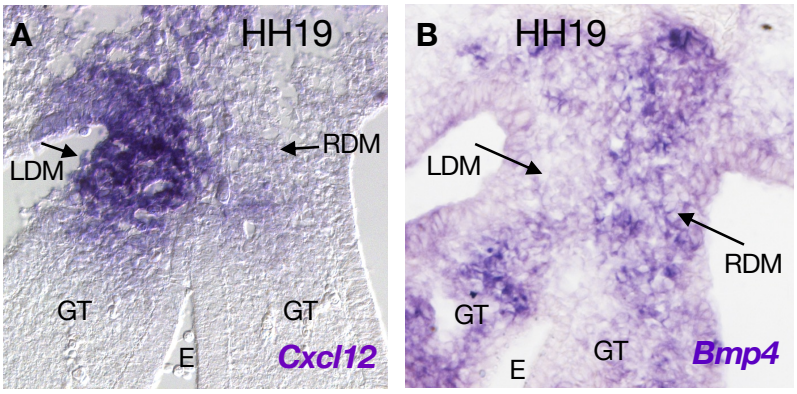

Hypothesis for role of midline in signal segregation

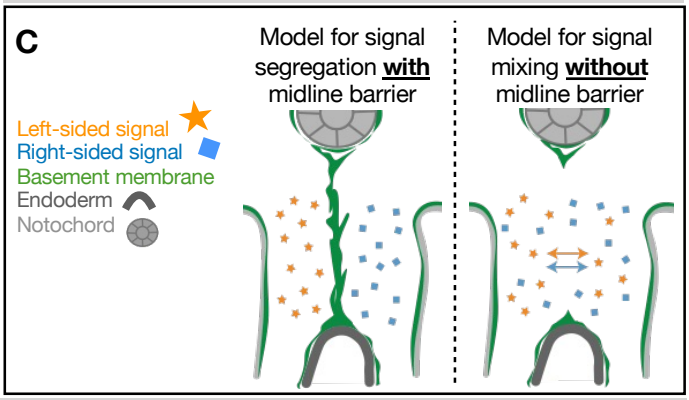

Dextran diffusion across the midline is prevented when the midline is intact

Midline intact, diffusion prohibited

Midline fragmenting, some diffusion in most embryos

Midline absent, diffusion permitted

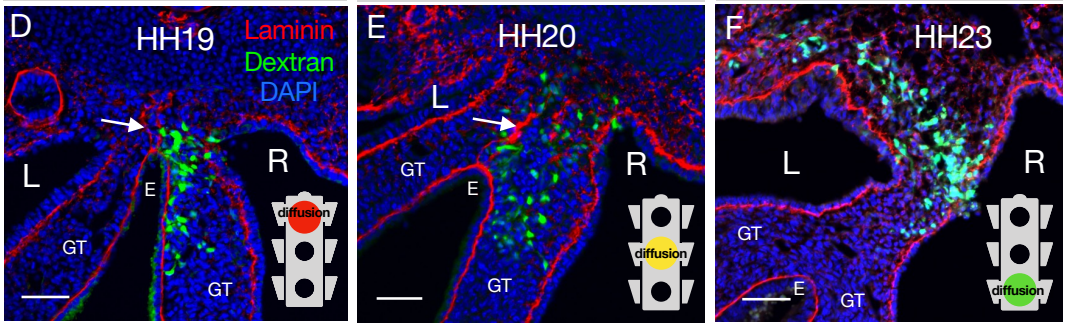

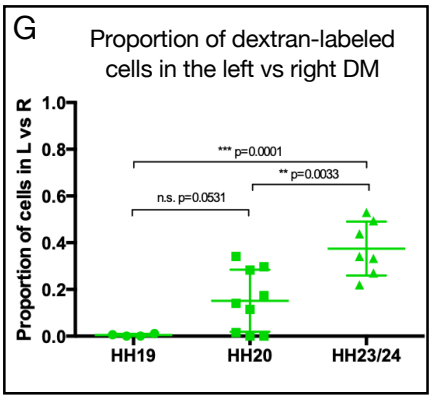

AMD3100-BODIPY diffusion across the midline is prevented when the midline is intact

Midline intact, diffusion prohibited

Midline absent, diffusion permitted

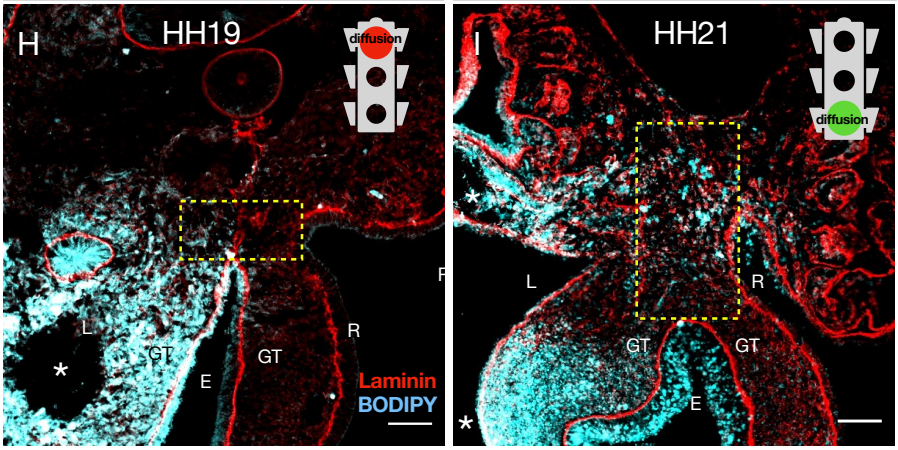

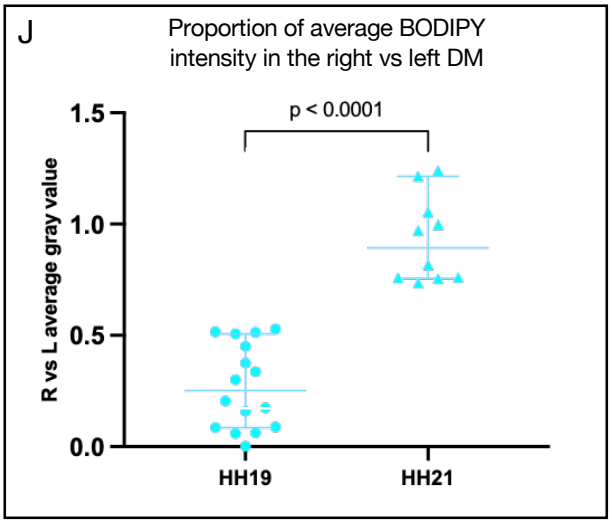

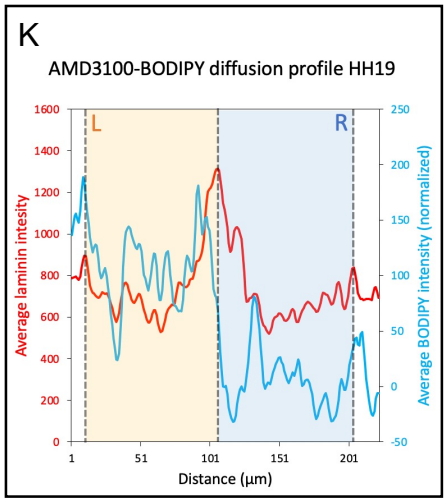

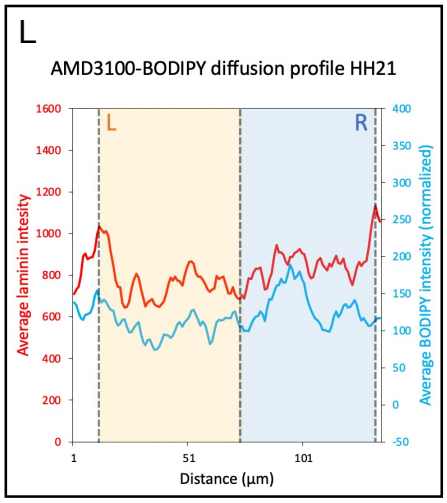

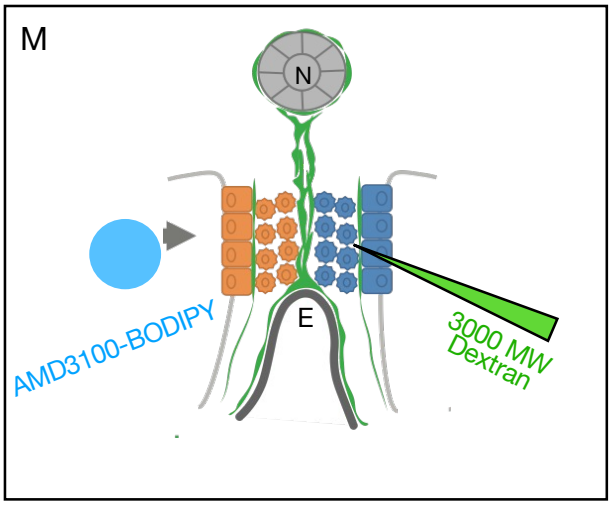

FIGURE 6

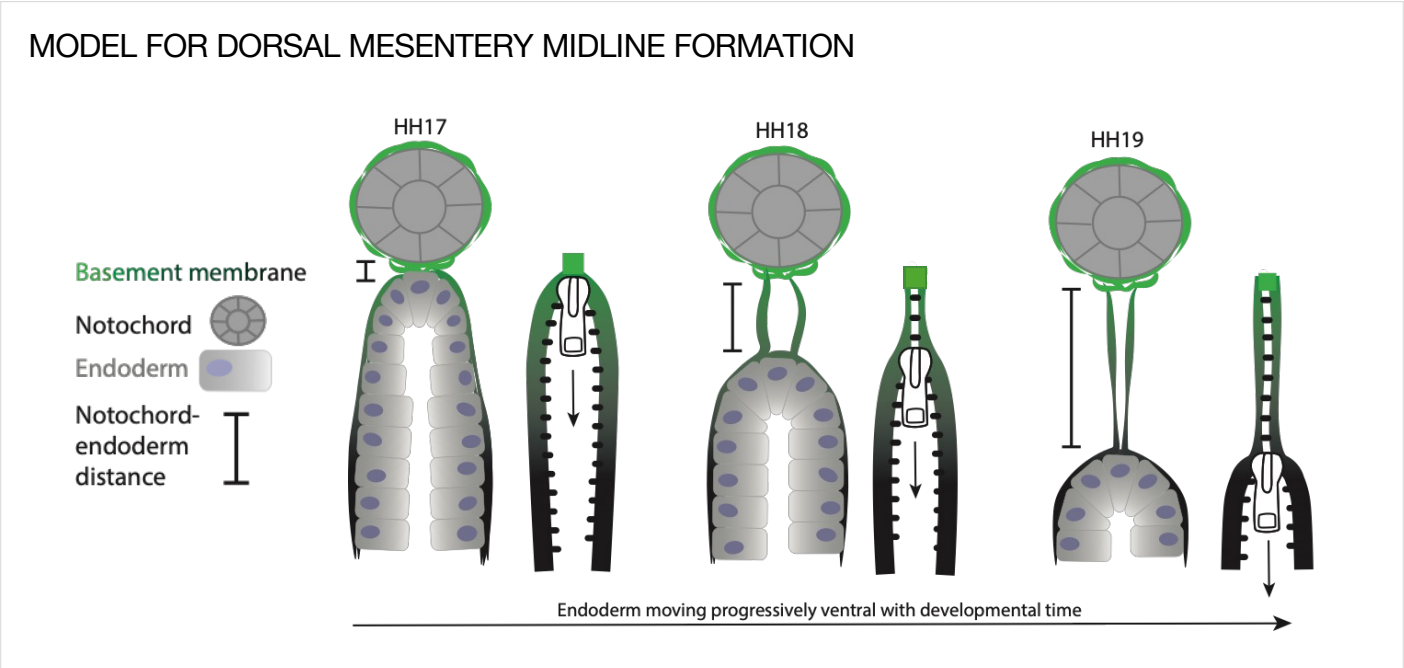
MODEL FOR DORSAL MESENTERY MIDLINE FORMATION
HH17
HH18
HH19
Basement membrane
Notochord
Endoderm
Notochord-
endoderm
distance
Endoderm moving progressively ventral with developmental time

FIGURE 7

Supplemental Figures

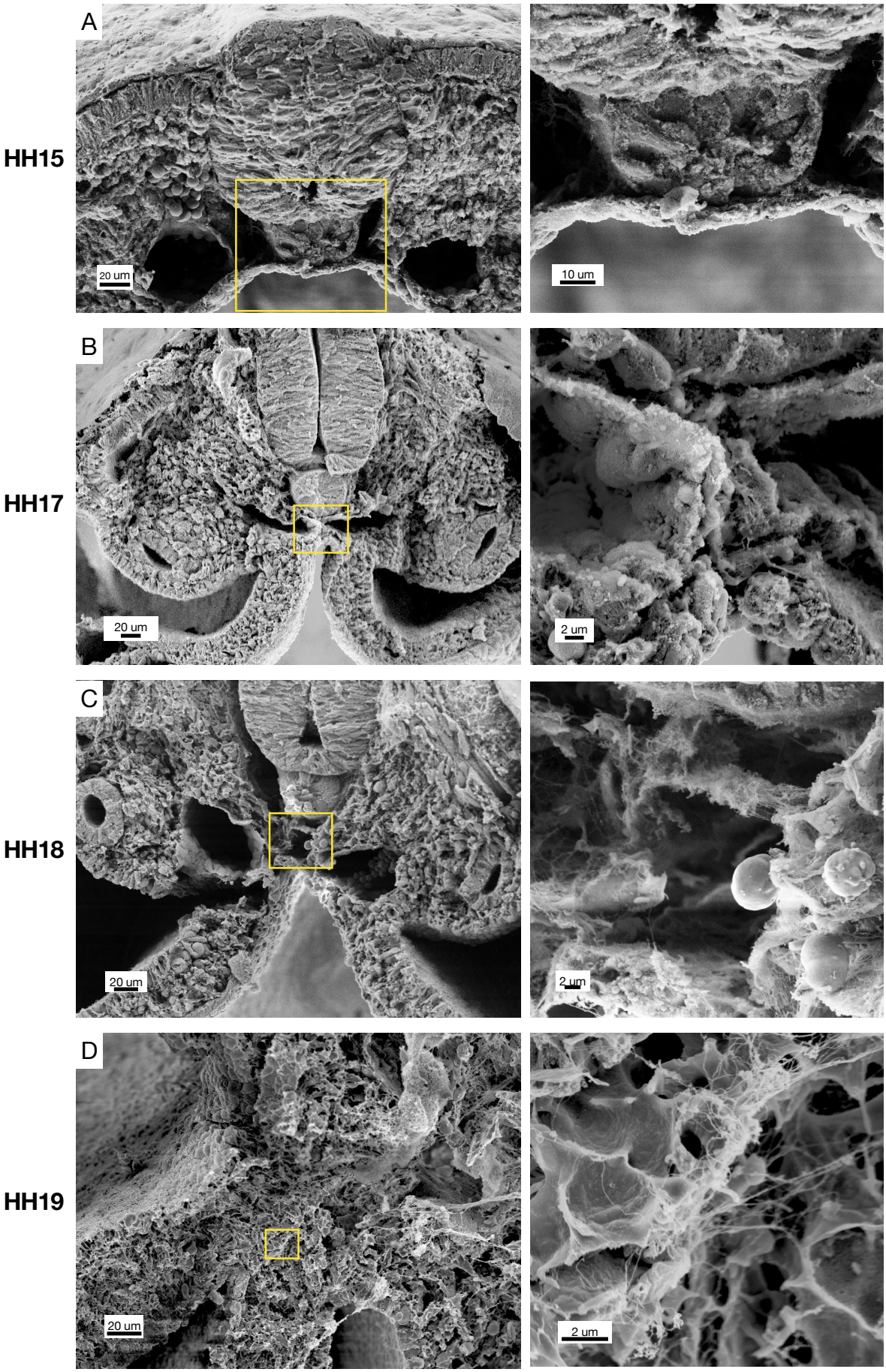

FIGURE S1

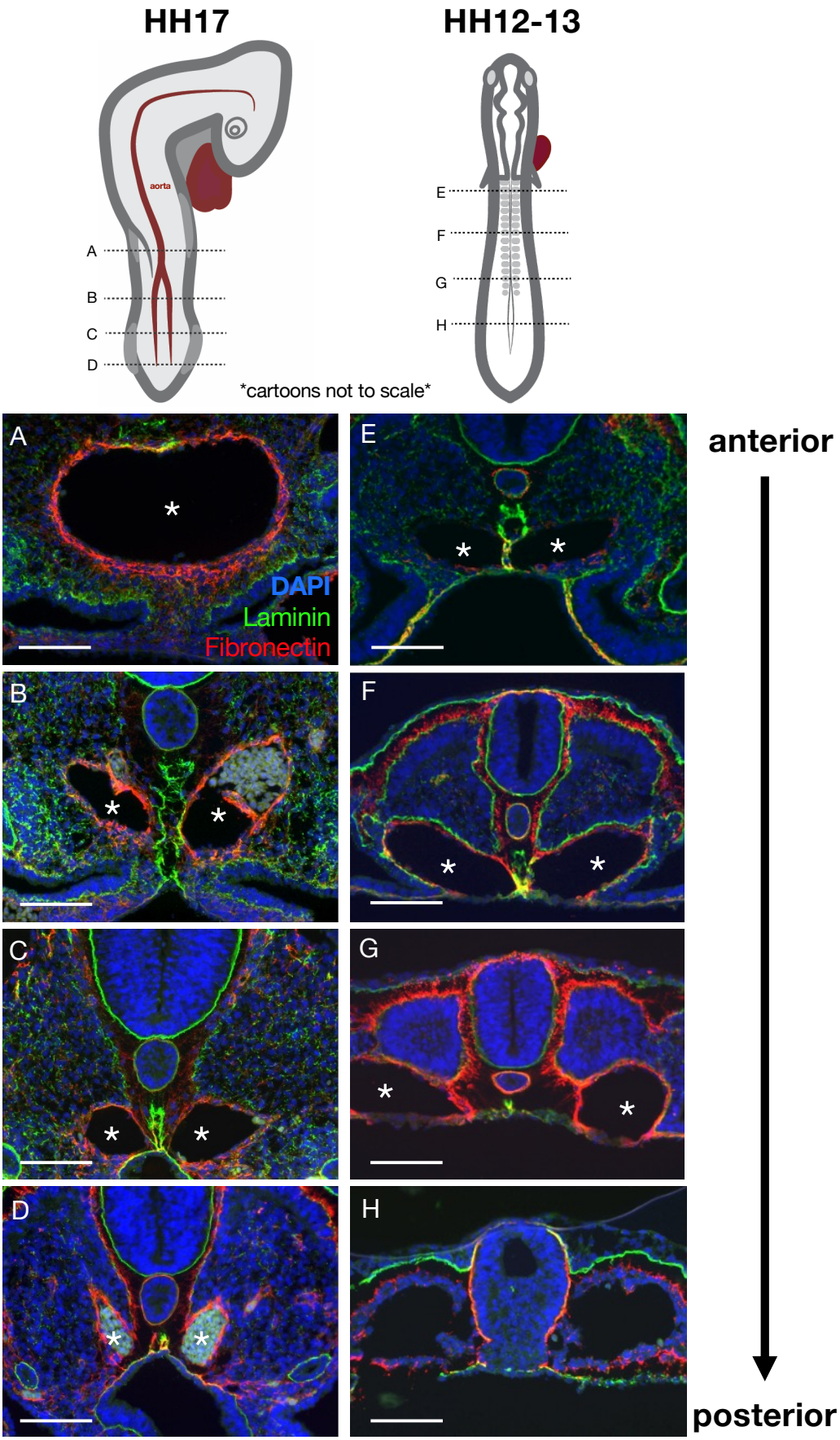
HH17
HH12-13
aorta
A
B
C
D
E
F
G
H
cartoons not to scale
DAPI
Laminin
Fibronectin
anterior
posterior

FIGURE S2

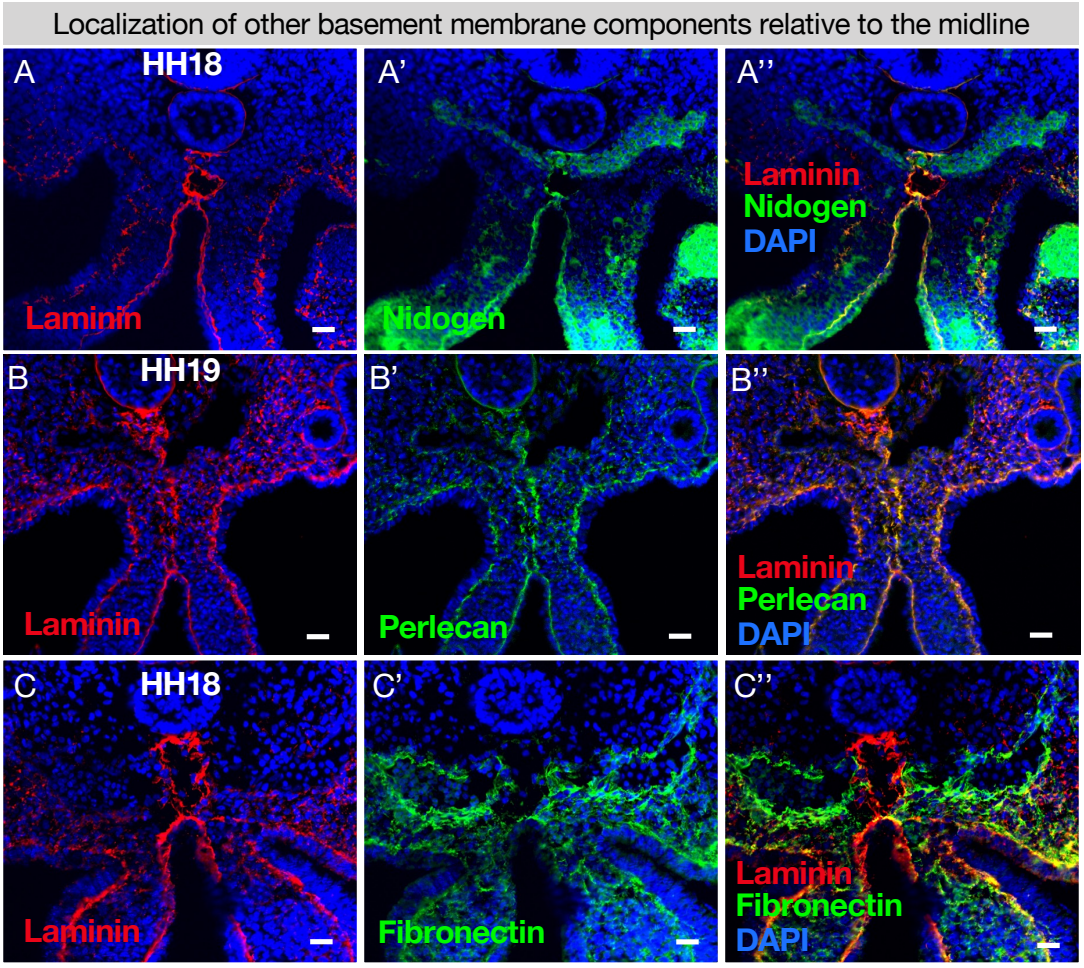
Localization of other basement membrane components relative to the midline
A
HH18
Laminin
A'
Nidogen
A''
Laminin
Nidogen
DAPI
B
HH19
Laminin
B'
Perlecan
B''
Laminin
Perlecan
DAPI
C
HH18
Laminin
C'
Fibronectin
C''
Laminin
Fibronectin
DAPI

FIGURE S3

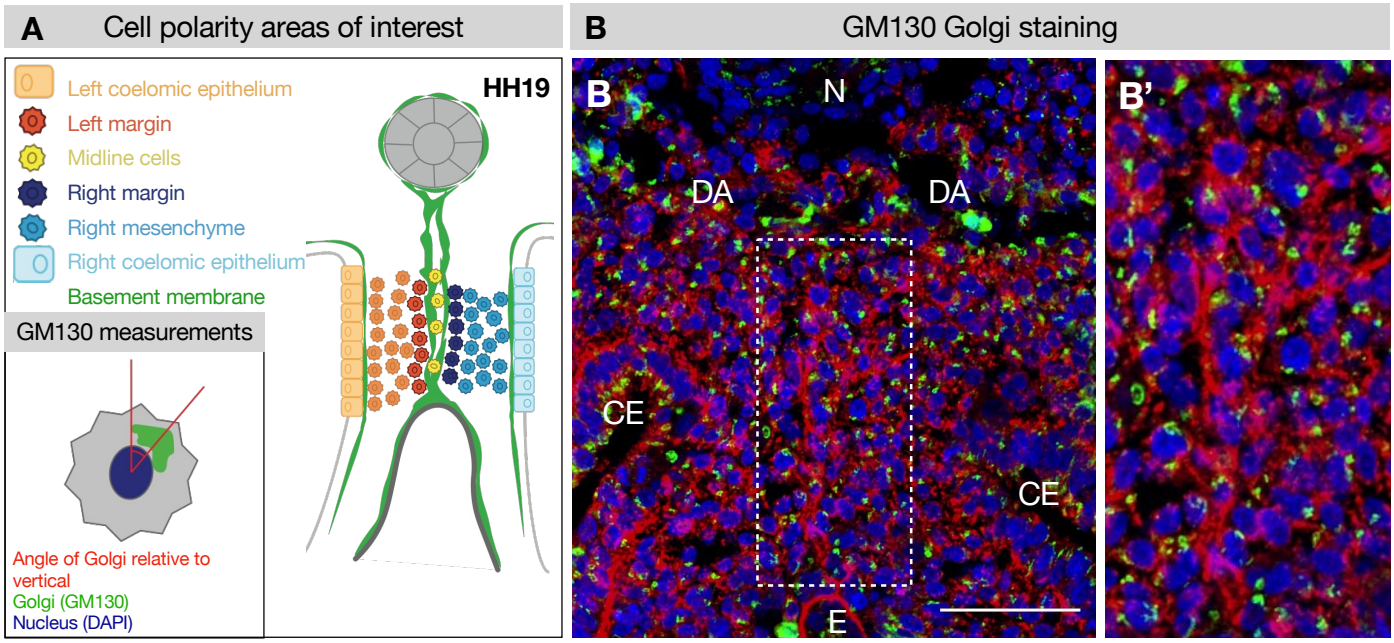
A
Cell polarity areas of interest
Left coelomic epithelium
Left margin
Midline cells
Right margin
Right mesenchyme
Right coelomic epithelium
Basement membrane
HH19
GM130 measurements
Angle of Golgi relative to vertical
Golgi (GM130)
Nucleus (DAPI)
B
GM130 Golgi staining
B
N
DA
DA
CE
CE
E
B'

FIGURE S4

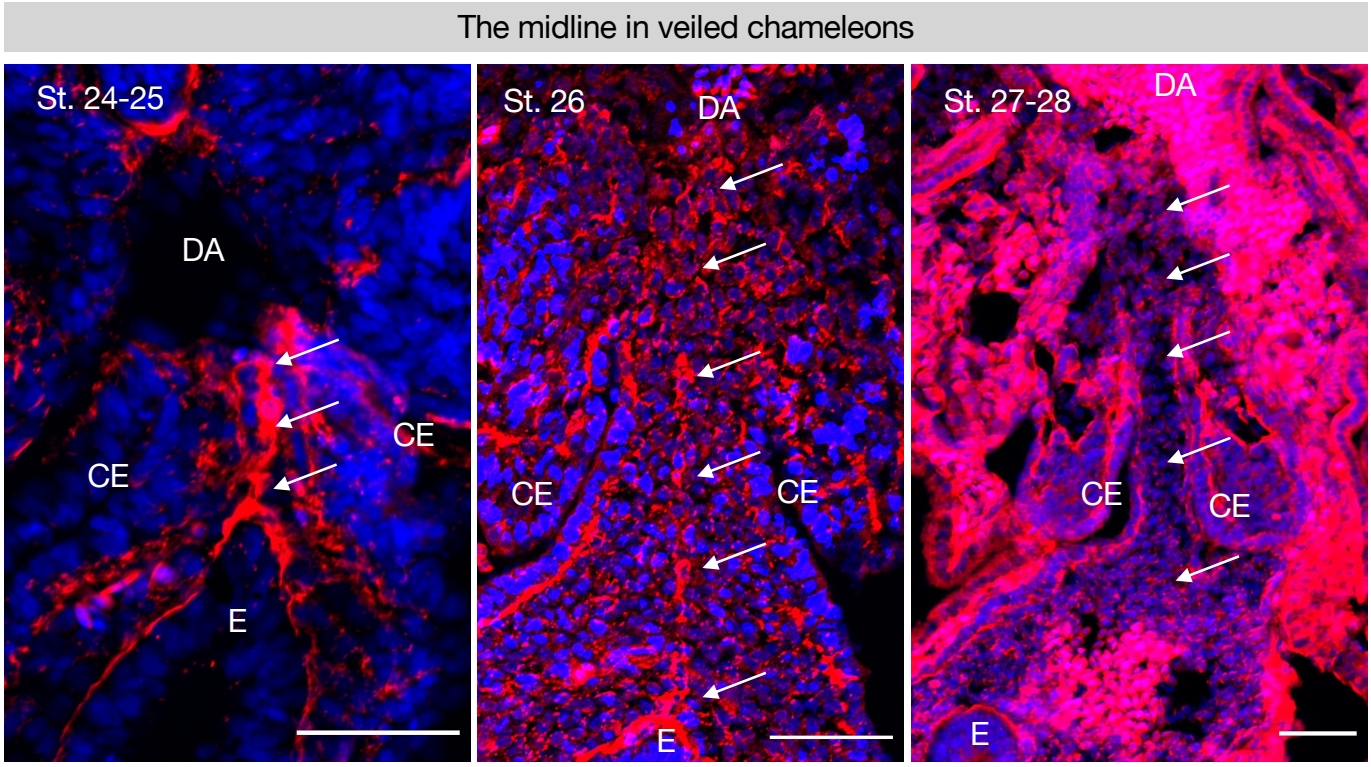
The midline in veiled chameleons
St. 24-25
DA
CE
CE
E
St. 26
DA
CE
CE
E
St. 27-28
DA
CE
CE
E

FIGURE S5